Department of Physics and Astronomy, University of Canterbury,
Private Bag 4800, Christchurch, New Zealand

Collateral Exposure:

The Additional Dose From Radiation Treatment

Katherine Fricker (BSc)

A thesis submitted in partial fulfilment of the requirements for the degree of Masters of Science at the University of Canterbury

MPHC 690 Thesis 2012

Supervisor: Juergen Meyer

Contents

List of Figures

List of Tables

Abstract

For patients receiving radiation therapy, there is a risk of developing radiation induced carcinomas, especially if they have a long life expectancy. However, radiotherapy is not the only contributor of radiation exposure to healthy tissue. With the introduction of highly conformal treatment techniques comes the increase in pretreatment imaging necessary to accurately target tumour volumes and consequently, radiation exposure to healthy tissue.

In this work the radiation dose delivered to radiosensitive organs from a number of treatment planning techniques was evaluated and the risk of radiation induced cancer was assessed. MOSFET detectors and Gafchromic film were used to measure the accumulative concomitant dose to the thyroid and contralateral breast from early stage breast carcinoma radiotherapy and to the contralateral testis from seminoma radiotherapy, with dose contributions from CT imaging for treatment planning, pretreatment imaging (CBCT) and treatment delivery peripheral dose. To the author's knowledge this is the first work investigating the total concomitant treatment related dose and associated risk to these treatment sites.

Peripheral dose contributed the largest concomitant dose to the healthy tissue, measuring up to 0.7, 1.0 and 5.0 Gy to the testis, thyroid and contralateral breast, respectively. The highest testicular, thyroid and contralateral breast carcinoma risk was found to be 0.4, 0.2 and 1.4%, respectively.

In conclusion, the risk of radiation induced carcinoma to the assessed radiosensitive tissues was found to be minimal, however, when considering treatment techniques and/or introducing pretreatment imaging protocols, the dose to the normal tissue should be kept as low as reasonably achievable.

Chapter 1

Introduction

Modern treatment techniques are capable of delivering highly conformal dose to target volumes and rely on image guidance to accurately target the tumour volumes. Inevitably, radiation is unintentionally delivered to normal tissue in the surrounding regions. This radiation dose comprises of scatter from within the patient, collimation scatter and radiation leakage through the head of the treatment machine and is herein collectively referred to as peripheral dose. Additionally, healthy tissue will receive dose contributions from beam entrance and exit dose, planning CT and pretreatment imaging. Dose to tissue from diagnostic medical exposure is in the order of mGy; e.g., 24 mSv for a chest Cone-beam CT (CBCT)[2] and 30 mGy for a adult chest CT scan[3], while from radiotherapy, healthy tissue can receive dose in the order of Gy[4,5].

The improving prognosis of radiation therapy is increasing the longevity of patients and thus the time in which treatment related side effects can occur. The risk of radiation inducing cancer is known from studying survivors of atomic bombs[6,7] and other incidences involving radioactive materials, e.g. Techa River[8]. More recently, the link between radiation exposure for medical purposes and cancer induction has been investigated[7,9].

An increased incidence of cancer, such as leukaemia[10], lung[11] and breast[12] to name a few, has been observed amongst patients who have received previous radiotherapy treatment compared with the general population. Furthermore, the associated incidence is age dependent and is greater for patients exposed at a younger age[12,13]. This correlation is not

limited to therapeutic doses. Brenner *et al.*[14] suggested that approximately 1.5% to 2.0% of all cancers in the United States may be related to the radiation dose from CT studies. Similarly, Berrington de González *et al.*[15] estimated that approximately 2% of the cancers diagnosed every year in the United States could be CT related.

An increased incidence of contralateral testicular cancer[16,17] and a reduction in sperm count[18] has been observed following radiotherapy for testicular seminoma and consequently, the dose to the contralateral testis is of concern. This dose has been investigated previously using thermoluminescent detectors[19] and several authors advocate the use of gonadal shielding to reduce the dose to the contralateral testis[19,20]. Similarly, the dose to the contralateral breast from breast carcinoma radiotherapy has been investigated[21–24] and the associated second cancer risk assessed. Additionally, the dose to the contralateral breast from diagnostic imaging (CBCT) has been measured using an ionisation chamber[25]. Although treatment and imaging related dose has been studied independently, to the author's knowledge, the total concomitant treatment related dose and subsequent secondary cancer risk has yet to been investigated.

The aim of this work is to assess the radiation induced cancer risk as a result of the total concomitant treatment related dose. The concomitant dose to the thyroid and contralateral breast from early stage breast radiotherapy and the dose to the contralateral testis from seminoma radiotherapy were measured using MOSFET detectors and Gafchromic film. Additionally, dose contributions from treatment related CT and Cone-beam CT (CBCT) imaging are considered.

In Chapter 2, the suitability of MOSFET and Gafchromic film for measuring these doses is discussed. Chapter 3 details the risk models used to assess the dose related second cancer risks. The seminoma and breast cancer case studies are presented in Chapters 4 and 5, respectively, with the overall findings discussed in Chapter 6.

Chapter 2

Dosimetry

2.1 Introduction

The amount of radiation dose healthy tissue receives during diagnostic imaging or radiation treatment should be kept as low as reasonably achievable to reduce normal tissue complications, without compromising treatment intent. This dose is often measured via phantom simulations[26] or in clinical settings[27], to ensure safe practice, using dosimeters, such as, ion chambers, thermoluminescent detectors (TLD)[26–28], MOSFETs[29,30] and more recently, radiochromic film[31]. In this work, MOSFET detectors and two types of radiochromic film were used to measure peripheral surface dose from megavoltage treatment beams and surface dose from kilovoltage imaging beams. The suitability of these dosimeters is discussed.

2.2 Gafchromic Film

2.2.1 Introduction

Gafchromic film (International Speciality Products (ISP), Wayne, NJ) is a type of self developing radiochromic film, which since it's introduction in 2004, is gaining popularity as a suitable dosimeter in radiology[32–34] and radiation oncology[35–37] applications. Unlike traditional film, it is self processing and does not require handling in a dark room. Gafchromic film is versatile; it can be easily cut, immersed in water[38] and handled in room light[39]. In

this work two types of Gafchromic film were used to measure dose from imaging modalities and radiotherapy; XR-QA2 and EBT2, respectively.

EBT2 Gafchromic

EBT2 Gafchromic film was designed for use in the energy range 50 kiloelectron volt (keV) into megavolt (MV) and with sensitivity down to 1 cGy. The upper dose limit is 10 Gy if measuring in the red channel.[1]. It is near tissue equivalent (z_{eff}= 6.84), has high spatial resolution and exhibits weak energy dependence[40]. The film contains an active layer (Figure 2.1) with particles that polymerise and turn blue when exposed to ionising radiation. A yellow marker dye is incorporated into the active layer of the film which protects the active component from exposure to visible and UV light. Additionally, the dye can be used to improve dose accuracy, if measured on a colour scanner, by applying corrections for the non-uniformity in the film thickness.

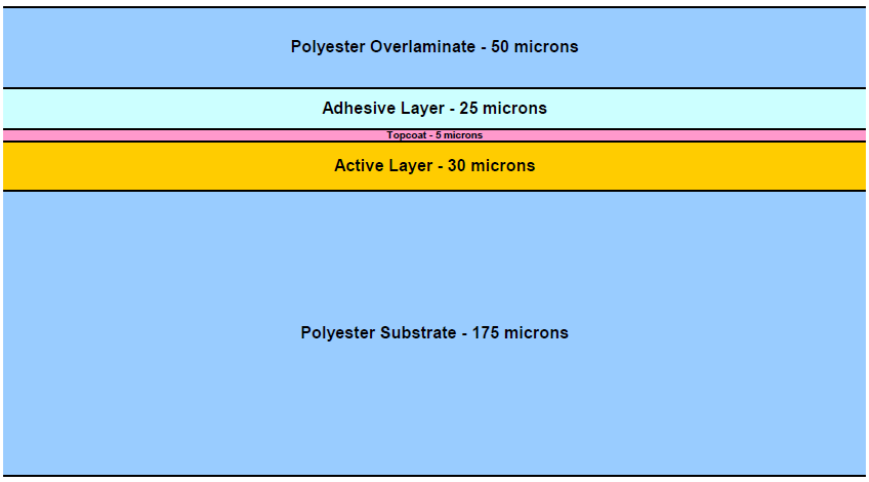

Figure 2.1: The composition of EBT2 Gafchromic film[1].

The film is digitised on a flatbed scanner[39,41,42] and the absorbed dose is determined by analysing the optical density of the film with respect to dose. The greatest uncertainty in the dose measurements is due to the scanning technique used, however, this can be reduced significantly if a rigorous scanning protocol is adhered to[42–44]. The film continues to darken over time after irradiation and the darkening behaviour is dose dependent[42,44]. To overcome this, it is recommended that the post irradiation scan time of the calibration and measurement films be kept consistent. Devic *et al.*[45] showed that a 1% dose error

can be achieved if a scanning window of ±2h is employed for a 24h post irradiation scan time. The uniformity of the scanner factors into the film response; differences of up to 5.5% have been reported depending on the position of the film on the scanner bed[42]. The orientation of the polyester substrate layer (i.e., facing towards or away from the glass) has little effect on the optical density for doses higher than 1 Gy (less than 1%)[39]. Alternatively, scanning in the portrait orientation produces variations of up to 9%[39]. In this work, a strict scanning protocol relating to film position, orientation and post irradiation digitisation time was maintained.

XR-QA2 Gafchromic

XR-QA2 Gafchromic film is radiochromic film designed for dosimetric use in the energy range 20 - 200 kVp and within the recommended dose range 0.1 - 20 cGy. It has a strong energy dependence in the kV range and the sensitivity of the film response increases for radiation beams in the higher kV energy range[46]. For the same dose, Rampado *et al.*[46] reported a film response 72% lower for 28 kVp compared to 120 kVp. In the higher energy range (80 - 140 kVp), the maximum variation was less than 20%. The post-exposure film darkening is most significant in the 24 hours after irradiation, although, small variations have been found up to 4 days after exposure[46]. Similarly, a rigid scanning protocol was used when digitising XR-QA2 film.

2.2.2 Calibration Procedure

EBT2 film calibration

Gafchromic EBT2 film has been shown to have little energy dependence in the megavoltage energy range[47] however, individual film calibrations were determined for the dose range 0 - 166 cGy for all energies used, namely, 6, 10 and 18 MV. Film calibration was carried out on a Varian iX linear accelerator (Varian Medical Systems, Palo Alto, CA). The majority of measurements were made for doses less than 50 cGy to ensure accuracy in the film calibration at low doses. Gafchromic film (lot #:A10061001B, expiration date: October 2012) was cut

into 4 x 4 cm^2 pieces and marked to keep the orientation of the film consistent. A film piece was placed in a 30 x 30 x 20 cm^3 stack of Solid Water® (Gammex RMI, Middleton, WI, USA) at a depth of 5 cm. The centre of the film was aligned with the central axis of the beam along the crosswires. The linear accelerator dose delivery is linear down to 3 Monitor Units (MU), where 1MU is defined as 1 cGy to D_{max} at a source to axis distance (SAD) of 100 cm, in a 10x10 cm^2 field. In order to ensure linearity of the beam at low doses, the solid water was placed at an extended SSD. The ratio of dose delivered at isocentre in a water phantom (10 x 10 cm^2 field, 95 cm SSD) to that at the extended SSD in solid water (5 cm depth, 5 x 5 cm^2, 200 cm SSD) was used to correct for the extended SSD setup. The correction factor, C_{ext}, accounts for the change in field size, SSD and any discrepancies between measurements made in the water and solid water phantoms. Twelve pieces of film were irradiated with 0, 1, 2, 3, 4, 5, 10, 20, 50, 100, 150 and 200MU, respectively. This was repeated three times.

The dose (D) to the films was calculated from the delivered MU, with adjustments made for the deviation of the machine output from calibration, O_c, which is the ratio between the current machine output and that at calibration, the placement of the film at depth and the extended SSD setup and is given by;

$$D = MU \times O_c \times TMR \times C_{ext}$$

The Tissue Maximum Ratio (TMR) at a depth of 5 cm was 0.918, 0.956 and 0.990 for 6, 10 and 18 MV, respectively. The applied doses to calibrate EBT2 film in 6, 10 and 18 MV beams are given in Table 2.1.

Table 2.1: The dose applied for calibration of EBT2 film ranged 0 - 166 cGy.

Applied Dose (cGy) for Film Calibration												
	Monitor Units (MU)											
Energy	0	1	2	3	4	5	10	20	50	100	150	200
6 MV	0.0	0.8	1.5	2.3	3.0	3.8	7.5	15.1	37.7	75.4	113.1	150.8
10 MV	0.0	0.7	1.5	2.2	2.9	3.6	7.3	14.5	36.3	72.6	108.9	145.2
18 MV	0.0	0.8	1.7	2.5	3.3	4.1	8.3	16.6	41.4	82.8	124.2	165.6

The film pieces were digitised one at a time using an Epson Expression 10000XL scanner (Seiko Epson Corporation, Nagana, Japan) 24±1 h post irradiation. Films were placed at the centre of the scanner bed, in a consistent landscape orientation, with the short edge of the original film parallel to the scanning direction and the polyester substrate layer facing the glass. The scanner was used in *professional mode*, with software selections *transmission* and *positive film* and with all filters and colour corrections turned off. Images were acquired in 48-bit colour, using a resolution of 72 dpi and saved in tagged image file format (TIFF). The scanner was switched on 30 minutes prior to use and a preview, followed by three scans to warm up the scanner before film digitisation commenced[48,49]. Additionally, a preview scan was performed prior to each scan[49]. Gloves were worn at all times when handling the film. The image files were imported into MATLAB® (MATLAB R2011a, The MathWorks Inc., Natick, MA) and the central 58 x 58 pixels (2 cm^2) were extracted and separated into red, blue and green channels. Care was taken to exclude any film area within 0.5 cm from a cut film edge. A correction, recommended by the manufacturers, was applied to the red channel data to smooth out possible inconsistencies in the thickness of the active layer[50]. The pixel values were converted to optical density as follows:

$$OD = -log_{10}(pixelvalue/65535)$$

For each film piece, the mean optical density of the corrected red channel data was plotted against the applied dose to establish the calibration curve. The mean of the three calibration curves was used for film analysis (Figure 2.2). For all EBT2 dosimetry measurements, the above scanning protocol was used and unless stated otherwise, the central 0.5 x 0.5 cm^2 (14 x 14 pixels) was extracted for film analysis. Figure 2.3 illustrates the weak energy dependence of EBT2 film in the MV energy range.

The maximum uncertainty (2SD) of any point in the calibration curves was 2.0, 1.4 and 1.4% for 6X, 10X and 18X, respectively.

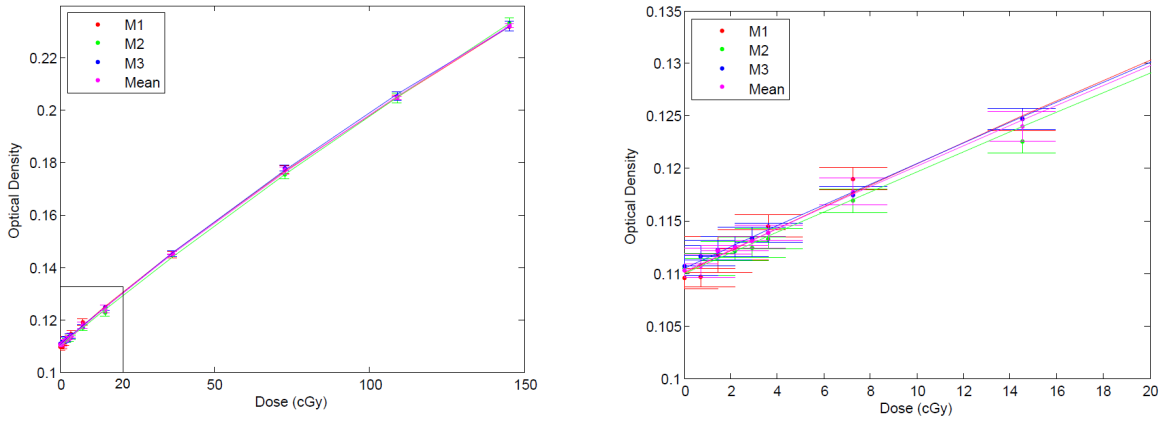

(a) Dose range 0 - 150 cGy

(b) Dose range 0 - 20 cGy

Figure 2.2: Red channel response for three sets of film irradiated to determine the 6 MV calibration curve. The mean of the three measurements is also given (magenta).

XR-QA2 film calibration

XR-QA2 Gafchromic film was calibrated for measuring surface dose from Cone-beam CT and CT image acquisition. Because of the strong energy dependence of the film in the kV energy range, the beam qualities of the fore mentioned imaging modalities were determined prior to calibration. The X-ray beam qualities of an On-Board Imager® (OBI) v1.4 and cone-beam CT capable Varian Linear Accelerator were measured for the standard CBCT protocols (100,

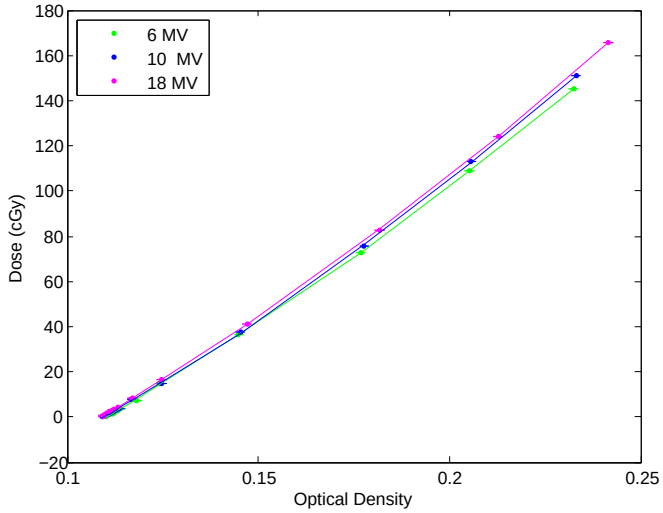

Figure 2.3: Calibration curves for EBT2 Gafchromic film for beams of different megavoltage energies.

110 and 125 kVp). Clinically, an aluminium compensator (bowtie filter) is introduced into the beam path to reduce the dose to the patient and improve image quality[51,52]. To assess the greatest range of Half Value Layers (HVLs) the full bowtie filter was fitted. A Piranha multimeter (RTI, Sweden) was used to evaluate the effects of the bowtie filter on HVLs on the central axis and at longitudinal displacements up to 10 cm. The HVLs ranged 4.9 - 7.6 mm Al (mean HVL = 6.3 mm Al) over all assessed positions. The mean beam quality on the central axis from the 3 protocols was 5.5 mm Al. The HVL increased off axis due to beam hardening.

According to manufacturer's specifications, the Siemens Somatom Sensation Open helical scanner (Siemens Medical Solutions, Erlangen, Germany) HVL was 9.1 mm Al for a 120 kVp imaging protocol. The dose delivered by the OBI X-ray source is unknown without the aid of external dose meters and therefore, the OBI X-ray source is not suitable for calibrating dosimeters. To overcome this, XR-QA2 Gafchromic film was calibrated on an XStrahl 300 X-ray Therapy Unit (XStrahl Ltd., Surrey, UK) using a 150 kVp beam with beam quality HVL = 6.0 mm Al, similar to those expected during CBCT acquisition. A 180 kVp beam with beam quality HVL = 9.5 mm Al was used to calibrate the film for measurements on CT. The 150 and 180 kVp beams were calibrated in water under reference conditions, (30 cm SSD, 8 cm circle applicator for 150 kVp and 50 cm SSD, 10x10 cm^2 applicator for 180 kVp) using a NE2571 graphite cylindrical ionisation chamber (NE Technology Ltd, Reading, UK) with a calibration traceable to a Secondary Standard Dosimetry Laboratory and in accordance with the IAEA TRS 277 protocol[53].

Gafchromic XR-QA2 film (lot #:A10071002A, Expiration Date: October 2012) was cut into 4 x 4 cm^2 pieces and marked with reference to the initial film orientation. The film was placed on the surface of a 30 x 30 x 13 cm^3 Solid Water® phantom and the NE2571 ionisation chamber was placed at a depth of 2 cm in the solid water to record the dose at depth (Figure 2.4). The film was calibrated under the beam reference conditions (30 cm SSD, 8 cm circle applicator for 150 kVp and 50 cm SSD, 10x10 cm^2 applicator for 180 kVp), henceforth referred to as standard setup conditions. Ten pieces of film were irradiated with 0.0, 1.2, 2.2, 3.2, 5.2, 8.2, 10.3, 14.3, 17.3 and 20.4 cGy, respectively. This was repeated three times

for each energy. The delivered dose (D) to the film pieces was calculated from the recorded ionisation chamber dose (D_{ion}), with corrections made for measuring at depth, PDD, and in a Solid Water® phantom, C_p, and is given by:

$$D = \frac{D_{ion} \times C_p}{PDD}$$

The Percentage Depth Dose (PPD) at 2 cm for the given beams is $PDD_{150\ kVp} = 76.1\%$ and $PDD_{180\ kVp} = 84.7\%$. The difference between measurements made in water and Solid Water® is 4.1% ($C_p = 1.041$) and 3.7% ($C_p = 1.037$) for 150 and 180 kVp, respectively.

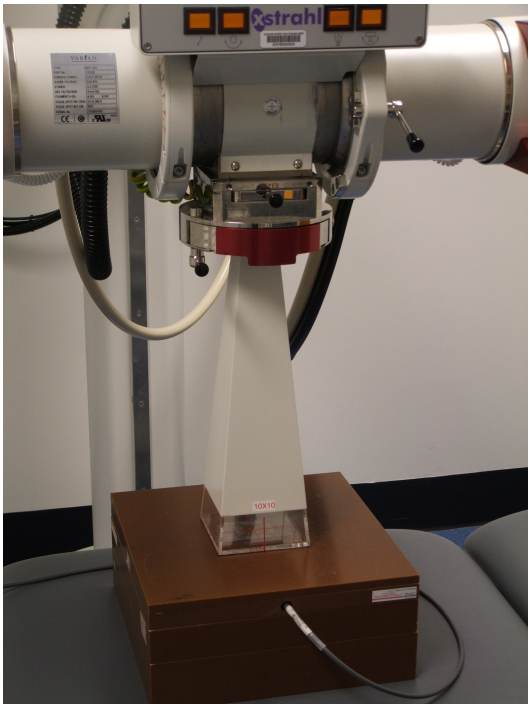

Figure 2.4: XR-QA2 film calibration in a 180 kVp beam with standard setup conditions.

Films were digitised on an Epson Expression 10000XL scanner in *reflection mode*, with software selection *professional mode*, photo and without any image corrections applied. Images were acquired in 48-bit colour, using a resolution of 72 dpi and saved in tagged image file format (TIFF). The scanner warm up procedure, handling of film and image manipulation were carried out as previously described for EBT2 film calibration. All XR-QA2 film was digitised in this manner, with the central 0.5 x 0.5 cm^2 (14 x 14 pixels) extracted for analysis of dosimetry measurements, unless stated otherwise.

The response of the film in the red, green and blue channels is illustrated in Figure 2.5.

The greatest sensitivity is observed in the red channel. The energy dependence of the film is visible in the kV energy range (Figure 2.6).

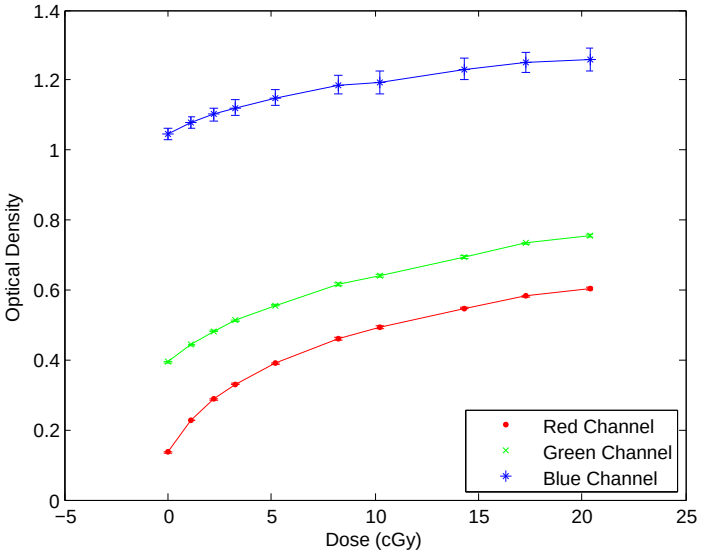

Figure 2.5: Red, green and blue channel response for one set of XR-QA2 film for beam energy 150 kVp.

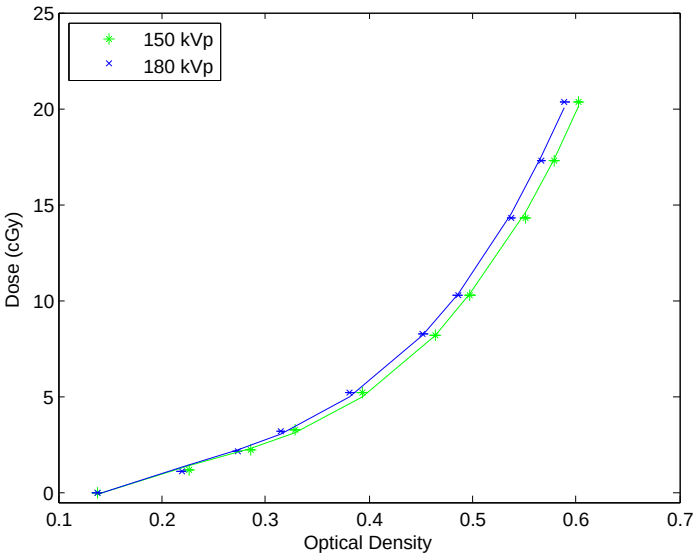

Figure 2.6: Calibration curves for XR-QA2 Gafchromic film for beam energies 150 and 180 kVp.

2.2.3 Uncertainty of Gafchromic Film

The reproducibility of EBT2 and XR-QA2 film with low dose delivery was assessed in MV and kV beams, respectively. A 3 x 3 cm^2 piece of EBT2 was placed in a 30 x 30 x 20 cm^3 stack of solid water (95 cm SSD) at a depth of 5 cm. A total of 20 pieces were exposed to 5 cGy in a 6 MV beam. The mean dose to the central 0.5 x 0.5 cm^2 was evaluated. The measurement error increases rapidly for doses below 1 cGy in kilovoltage beams. Additionally, the error was dependent on the energy of the beam[46]. For assessment in kilovoltage beams, a 3 x 3 cm^2 piece of XR-QA2 film was positioned on the surface of a 30 x 30 x 13 cm^3 stack of solid water in standard setup conditions for 150 and 180 kVp. For each kV beam, 20 film pieces were exposed to 2 cGy. The uncertainties (2 SD) in the measurements are given in Table 2.2.

Table 2.2: The reproducibility (95% CI) of Gafchromic film for low dose exposures.

Gafchromic Film Reproducibility (%)		
Energy	Applied Dose	
	2 cGy	5 cGy
150 kVp	3.1	-
180 kVp	3.0	-
6 MV	-	1.0

Despite the low applied dose, these findings are in agreement with previous reports[41,42,46]. Richley *et al.*[42] reported the uncertainty (2SD) of EBT2 to be 1.1 - 1.2% for applied doses 50 - 300 cGy with a 6 MV beam. In another study, the uncertainty (2SD) was reported as 2.4, 3.0 and 3.0% for applied doses with a 6 MV beam of 100, 200 and 300 cGy[41]. Rampado *et al.*[46] determined that for an applied dose of 2 cGy with a 140 kVp beam, the uncertainty (2SD) of XR-QA2 was 6%.

2.3 Metal Oxide Seminconductor Field Effect Transistors (MOSFET)

2.3.1 Introduction

Metal oxide semiconductor field effect transistor (MOSFET) detectors are widely used for clinical dosimetry[29,30,54,55]. They are highly sensitive, show little energy dependence in the MV energy range[56] and their small size and direct reading capability provides ease of use. The operating principles of MOSFET detectors have been described previously[57,58]. Essentially, a MOSFET consists of P-type silicon substrate, an oxide layer and a metal gate. Ionising radiation creates charge in the silicon oxide layer resulting in a shift in the gate voltage (threshold voltage). The shift allows charge conduction through the MOSFET and is proportional to the dose deposited in the oxide layer.

Several authors have investigated the angular dependence of MOSFETs. Chuang *et al.*[30] reported angular dependence of $\pm 2.5\%$ for 6 MV beams, while Ehringfeld *et al.*[59] found angular dependence of $\pm 5.0\%$ for 180 kVp and 250 kVp beams. This increased significantly, $> \pm 20\%$, for 100 kVp. Other limitations include large energy dependence in the kV range[59] and a limited life time, usually around 20,000 mV.

In this work, measurements were made using high sensitivity TN-1002RD MOSFETs (Thomson & Nielsen, Ottawa, Canada), with a high bias setting, in conjunction with the AutoSense System.

2.3.2 Calibration Procedure

MV calibration

The energy dependence of MOSFETs in the megavoltage energy range ^{60}Co - 15 MV is reported to be 5%[56]. Despite the weak energy dependence, individual calibration factors were determined for 6, 10 and 18 MV beams. MOSFETs were positioned with the black bulb down (away from the beam), as per manufacturer's recommendations, in a MOSFET specific Perspex phantom created in the workshop at Auckland DHB (Figure 2.7). The

phantom accommodates up to five MOSFETs. The Perspex phantom was placed on the treatment couch at 100 cm SSD, with at least 10 cm Solid Water® for backscatter, in a 10 x 10 cm^2 field. 5 cm of Solid Water® was placed on top of the Perspex phantom for build up.

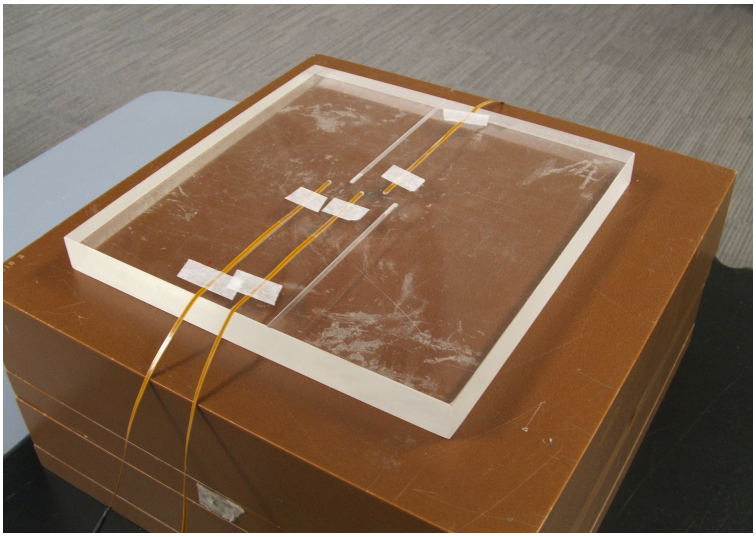

Figure 2.7: The Perspex MOSFET phantom. The grooves accommodate the raised black bulb and allow up to five MOSFETs to be calibrated simultaneously.

As recommended by the manufacturers, the MOSFETs were irradiated with sufficient dose to cause a minimum 200 mV shift in the threshold voltage. The MOSFETs were read out immediately. Five consecutive measurements were made ensuring at least five minutes passed between each irradiation. This calibration process was carried out for all energies as required or at approximate threshold voltages 0, 10,000 and 15,000 mV. The dose (D) applied was calculated from the delivered MU with adjustments made for the deviation of the machine output from calibration O_c and the placement of the MOSFETs at depth and follows as:

$$D = MU \times O_c \times TMR$$

The Tissue Maximum Ratio (TMR) at a depth of 5 cm is 0.918, 0.956 and 0.990 for 6, 10 and 18 MV, respectively.

The CF were determined from the mean of the five measurements:

$$CF = \frac{\overline{m_i}}{D}$$

Where m_i is the MOSFET reading in millivolts (mV).

The mean CF for 6, 10 and 18 MV was 785.0 ± 11.3 mV/Gy, 784.8 ± 10.3 mV/Gy, 773.9 ± 11.7 mV/Gy, respectively. The variation in CF across the MV energy range assessed was 1.4%. However, individual detector calibration factors were used.

kV calibration

MOSFET detectors were calibrated two at a time using the XStrahl 300 X-ray Therapy Unit. Calibration factors (CF) were determined for 150 and 180 kVp beams. Two MOSFETs were placed on the surface of a solid water phantom (30 x 30 x 13 cm^3) in standard setup conditions (Figure 2.8), with the black bulb facing upwards (as recommended by the manufacturers for kilovoltage energies), at a lateral displacement ±0.5 cm from the central axis. A NE2571 graphite cylindrical ionisation chamber was placed at a depth of 2 cm to measure the delivered dose. No interference in the ionisation chamber measurements was expected due to the presence of the MOSFETs since they were laterally displaced. The MOSFETs were irradiated with sufficient dose to result in a minimum signal of 200 mV, as suggested by the manufacturers. Five measurements were recorded allowing at least five minutes between each irradiation. The dose (D) delivered to the MOSFETs was calculated from the ion chamber measurements, D_{ion}, with corrections applied for measuring in solid water and at depth and is given by;

$$D = \frac{D_{ion} \times C_p}{PDD}$$

The Percentage Depth Dose (PPD) at 2 cm for the given beams was $PDD_{150\ kVp} = 76.1\%$ and $PDD_{180\ kVp} = 84.7\%$. The difference between measurements made in water and Solid Water® was 4.1% ($C_p = 1.041$) and 3.7% ($C_p = 1.037$) for 150 and 180 kVp, respectively.

The calibration factors were determined as previously described (equation 2.3.2). The mean CF was 25.1 ± 0.7 mV/cGy and 23.7 ± 0.3 mV/cGy for 150 and 180 kVp, respectively. A slight energy dependence was observed; the kV calibration factors differed by 5.7%. The difference between detector calibration factors for the same energy was up to 14.4%. This agrees with the findings of Enringfeld *et al.*[59], who observed variations in detector calibration factors greater than 10% for energies below 180 kVp. This highlights the importance of using

individual calibration factors.

2.3.3 Uncertainty of MOSFETs

Several authors have reported on the uncertainty of metal oxide semiconductor field effect transistors for doses typical in a treatment fraction. For a dose delivery of approximately 1 Gy in a 6 MV beam, Gopiraj *et al.*[56] determined the reproducibility of low and high sensitivity MOSFETs to be 1.4% and 2.0% (1SD), respectively. Bulinski *et al.*[60] evaluated the reproducibility of MOSFETs in a 6 MV beam for a range of doses (17 - 100 cGy). The standard deviation was 3.7% for the lowest applied dose and 0.9% for the highest. Ehringfeld *et al.*[59] investigated the reproducibility of multiple MOSFET detectors (standard sensitivity, standard bias sensitivity) with energies 80 - 250 kVp and applied doses 0.2 - 2.5 Gy. The largest deviation, ±7.4%, was observed for applied doses equal to or less than 1 Gy. The maximum deviation for doses between 1.5 and 2 Gy was ±2.5% and for applied doses of 2.5 Gy, ±1%. Cheung *et al.*[61] reported the repeatability of a MOSFET for 50 consecutive irradiations of applied dose 100 cGy with a 250 kVp beam to be 2.6% (2SD of mean).

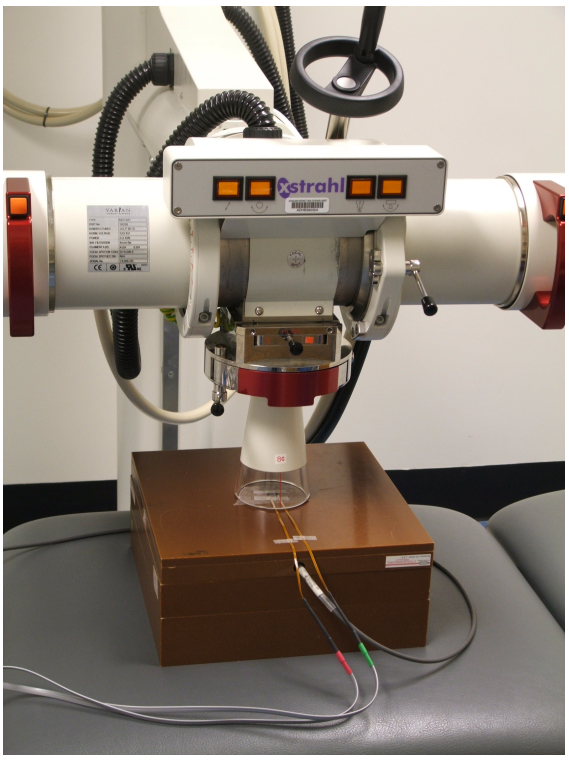

Figure 2.8: MOSFET detector calibration in a 150 kVp beam with standard setup conditions.

However, reports on the reproducibility of MOSFETs for doses less than 20 cGy, which are common in the periphery of treatment fields and in imaging fields, are scarce in the literature.

The reproducibility of high sensitivity TN-1002RD MOSFETs with low dose delivery was assessed in MV and kV beams. Four MOSFETs were placed in the MOSFET Perspex phantom, positioned centrally in a 10 x 10 cm^2 field (100 cm SSD, 2 cm depth), on a 30 x 30 x 10 cm^3 block of solid water. A total of 12 readings were recorded for an exposure of 2 and 5 cGy in a 6 MV beam. For evaluation in kilovoltage beams, two MOSFETs were positioned on the surface of a 30 x 30 x 13 cm^3 stack of solid water in standard setup conditions for 150 and 180 kVp. A total of 20 measurements were recorded for an exposure of 2 cGy. The uncertainties (2 SD) are given in Table 2.3. The reproducibility of MOSFET detectors for measuring low dose is poor for all energies investigated, with measurement uncertainties measurement of up to 54%. Despite this, the nominal dose inaccuracy is approximately 1cGy.

Table 2.3: The percentage uncertainty (95% CI) in high sensitivity MOSFETs for low dose exposures.

MOSFET Reproducibility		
Energy	Applied Dose	
	2 cGy	5 cGy
150 kVp	26.6	-
180 kVp	50.4	-
6 MV	53.6	18.1

2.4 Comparison of Dosimeters

The dose response of MOSFETs and Gafchromic Film (hereafter referred to as the dosimeters) was investigated to determine the suitability of using these dosimeters in primary kilovoltage (kV) and peripheral region of megavoltage (MV) beams. Dose in the peripheral regions of the MV treatment field is complex; with dose contributions from scatter within the patient (internal scatter), leakage from the head of the treatment machine (head leakage)

and collimator scatter. Internal scatter is the major contributor of dose in the near periphery of the treatment field, having spectra peaks near 500 keV, while head leakage dominates further a field[62]. The out-of-field dose is largely dependent on beam energy, field size and distance from the field edge[62–64]. The photon contribution decreases exponentially with distance from the field and the neutron contribution, which is significant for beam energies $\geq$ 15 MV, is independent of distance from the field but decreases with depth in tissue[65]. All these factors influence the choice of appropriate dosimeter to quantify peripheral dose.

2.4.1 Megavoltage Beam

MOSFET and Gafchromic film measurements were compared to those made with an IBA CC13 ionisation chamber (IBA Dosimetry, Beijing, China) which, due to low angular dependence and weak energy dependence across a broad spectrum (100 kVp to 50 MV), is a suitable reference dosimeter for out of field measurements. The dose response of the dosimeters under investigation was performed using a Varian iX 6 MV beam with the response to higher energies assumed to be similar since the energy dependence of EBT2 and MOSFETs is small in the MV energy range[47,56].

The response of the CC13 ionisation chamber and UNIDOS electrometer system (PTW, Freiburg, Germany) was established for the delivery of a range of doses (1.9 - 186.2 cGy). A Scanditronix-Wellhöfer water phantom system (Scanditronix-Wellhöfer, Uppsala, Sweden) was set up with the CC13 ionisation chamber positioned at a depth of 5 cm in a 10x10 cm^2 field, at 95 cm SSD. The mean of two readings were recorded for each dose delivery.

Peripheral dose measurements were made at increasing distances from the edge of a 10x10 cm^2 irradiated field using the CC13 ionisation chamber with the effective point positioned on the surface of the water, 1 cm from the edge of the field. Two peripheral dose measurements were made for the dose delivery on the central axis of 101.4 cGy to d_{max}. Measurements were repeated at 2, 3, 4, 5, 6, 8 and 10 cm from the field edge and again at 3, 4, 5, 6, 8 and 10 cm for the delivery on the central axis of 202.9 cGy to d_{max}.

3 x 3 cm^2 pieces of EBT2 film were positioned on the surface of a 30 x 30 x 20 cm^3 stack of Solid Water® (95 cm SSD), at distances 1, 2, 3, 4, 5, 6, 8 and 10 cm from the edge of

a 10 x 10 cm^2 field. The sequence of film irradiation was such that the film pieces did not overlap and interfere with the recorded dose. Individual sets of film pieces were exposed to peripheral dose from dose deliveries on the cental axis to d_{max} of 101.6 and 203.3 cGy, respectively. These measurements were repeated three times and the film was digitised 24 hours later.

Eight MOSFETs were used to carry out the same measurement described above, with doses prescribed to d_{max} on the cental axis of 101.5 and 203.1 cGy, respectively. The MOSFETs were read out after each irradiation.

The mean (95% CI) of the measurements for each dosimeter was recorded (Table 2.4). The uncertainty in the CC13 ionisation chamber measurements was 1% as specified by the manufacturers. The measured values were normalised to the CC13 ionisation chamber water surface dose measurements at the respective distances. These values are compared in Figure 2.9.

Table 2.4: The peripheral dose measured by EBT2 and MOSFETs dosimeters at distances (D) from the edge of a 10 x 10 cm^2 field were compared to CC13 ionisation chamber measurements (Ion). Dosimeter measurements were made on the surface of a stack of solid water. Comparisons were made for applied doses of 101 and 203 cGy. The uncertainty in the ionisation measurements is 1%. All values are given in cGy.

Peripheral Dose Dosimeter Comparison						
	Applied Dose = 203 cGy			Applied Dose = 101 cGy		
D (cm)	Ion	MOSFET	EBT2	Ion	MOSFET	EBT2
1	-	14.23±2.08	15.14±0.61	7.43	6.59±1.32	8.04±0.87
2	-	12.20±2.06	12.13±0.45	5.67	6.04±0.44	5.69±0.42
3	9.33	8.60±0.38	10.30±1.49	4.58	4.28±0.60	5.63±0.95
4	7.83	7.43±0.62	9.09±1.17	3.91	3.76±0.44	4.10±0.15
5	6.62	6.59±0.81	7.64±1.08	3.36	3.40±0.52	3.79±0.25
6	5.80	3.42±0.73	6.94±0.98	2.82	1.29±1.59	2.94±0.45
8	4.45	2.12±1.08	4.47±0.18	2.15	0.27±0.43	2.04±1.00
10	3.64	2.53±2.29	4.31±0.21	1.74	1.45±1.01	2.44±0.51

Overall, EBT2 tended to overestimate the dose and MOSFETs tended to underestimate the dose. For measurements up to 5 cm from the field edge, MOSFET measurements were in better agreement with the CC13 ion chamber measurements (10% variation) compared to

those made with film (25% variation). However, at greater distances, where the scatter contribution is reduced, the accuracy of the MOSFETs decreased. This finding is in agreement with other studies[66,67]. The maximum variation from the CC13 ion chamber measurements was 2.4 and 1.3 cGy for MOSFETs and EBT2, respectively.

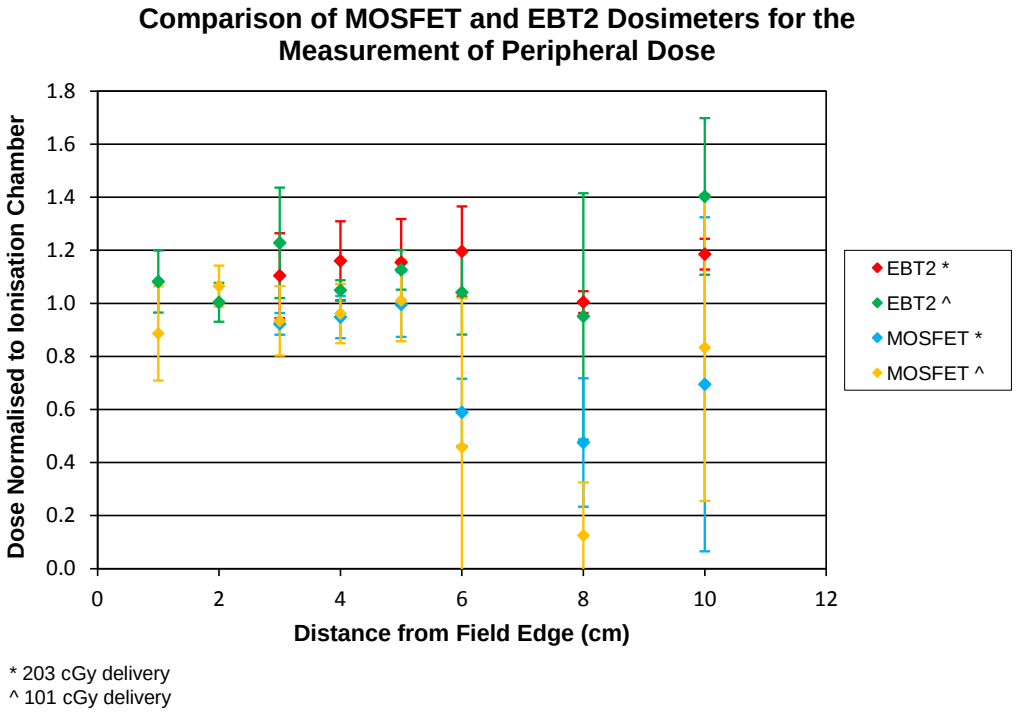

Figure 2.9: The comparison of EBT2 Gafchromic film and MOSFETs dosimeters for measurements in the periphery of a 6 MV beam. Doses were measured for a delivery of 101 and 203 cGy to d_{max} on the central axis of a 10x10 cm^2 field and normalised to those measured with a CC13 ionisation chamber.

2.4.2 Kilovoltage Beam

In order to accurately measure dose within CBCT and CT fields, the suitability of MOSFETs and XR-QA2 Gafchromic film for measuring dose within kV beams was determined. These imaging techniques have beam qualities equivalent to 150 and 180 kVp, respectively. The energy dependence of MOSFETs in the kilovoltage energy range is well known[59,67], exceeding 10% over the energy range 80 - 250 kVp. The energy dependence of XR-QA2 is approximately 10% over the range[68]. Consequently, the dose response of the dosimeters was compared with a NE2571 graphite cylindrical chamber for measurements made within both the 150 and 180

kVp beams. All measurements were performed using the XStrahl 300 X-ray Therapy Unit.

Two MOSFETs were positioned centrally on a stack of solid water, at least 10 cm high to ensure sufficient backscatter. The MOSFETs were displaced 0.5 cm lateral of the central axis to avoid interfering with the NE2571 ionisation chamber, which was placed at a depth of 2 cm on the central axis. Measurements were made under calibration conditions, i.e., 30 cm SSD, with an 8 cm circle applicator fitted for the 150 kVp beam and 50 cm SSD, with a 10 x 10 cm^2 applicator fitted for the 180 kVp beam. Measurements were made for a delivery of 1.1, 3.2, 5.2 and 10.3 cGy. The measurements were repeated three times and the MOSFETs were read out between each measurement, allowing at least 5 minutes between each irradiation.

Under the same conditions, three measurements were performed using XR-QA2 Gafchromic Film. The film was cut into 3 x 3 cm^2 pieces and fixed centrally using tape. The film was digitised 46 hours after irradiation.

The mean (95% CI) of the measurements is given in Table 2.5. The numerical values were normalised to the applied dose and the ratios are represented graphically in Figure 2.10.

Table 2.5: A comparison of the dose response of MOSFETs and XR-QA2 in kilovoltage beams of quality 150 and 180 kVp for the applied doses of 1.1, 3.2, 5.2 and 10.3 cGy as measured with the NE2571 graphite cylindrical chamber.

Dosimetric Response in Kilovoltage Beams				
	150 kVp		180 kVp	
Applied Dose (cGy)	MOSFET	XR-QA2	MOSFET	XR-QA2
1.1	1.12 ± 0.20	1.43 ± 0.02	0.81 ± 0.19	1.37 ± 0.02
3.2	3.26 ± 0.12	3.14 ± 0.02	2.90 ± 0.23	3.08 ± 0.02
5.2	5.47 ± 0.10	4.97 ± 0.01	4.97 ± 0.08	4.93 ± 0.02
10.3	11.25 ± 0.39	10.27 ± 0.01	10.33 ± 0.34	10.23 ± 0.07

XR-QA2 measures within 5% of the NE2571 ionisation chamber measurements for doses above 3 cGy but overestimates the dose by approximately 25% for a dose delivery of 1.1 cGy. This dose is approaching the limit of the recommended dose range 0.1 - 20 cGy. XR-QA2 film has excellent precision across the delivered dose range. MOSFET measurements are within 10% of the ionisation measurements for doses above 3 cGy. For a dose delivery

of 1.1 cGy, MOSFETs underestimate the dose on average by approximately 25% and 2% for measurements within the 150 and 180 kVp beam, respectively. The associated error is approximately 20%. Overall, MOSFETs and XR-QA2 are in good agreement (± 10%) with the NE2571 ionisation chamber for doses above 3 cGy.

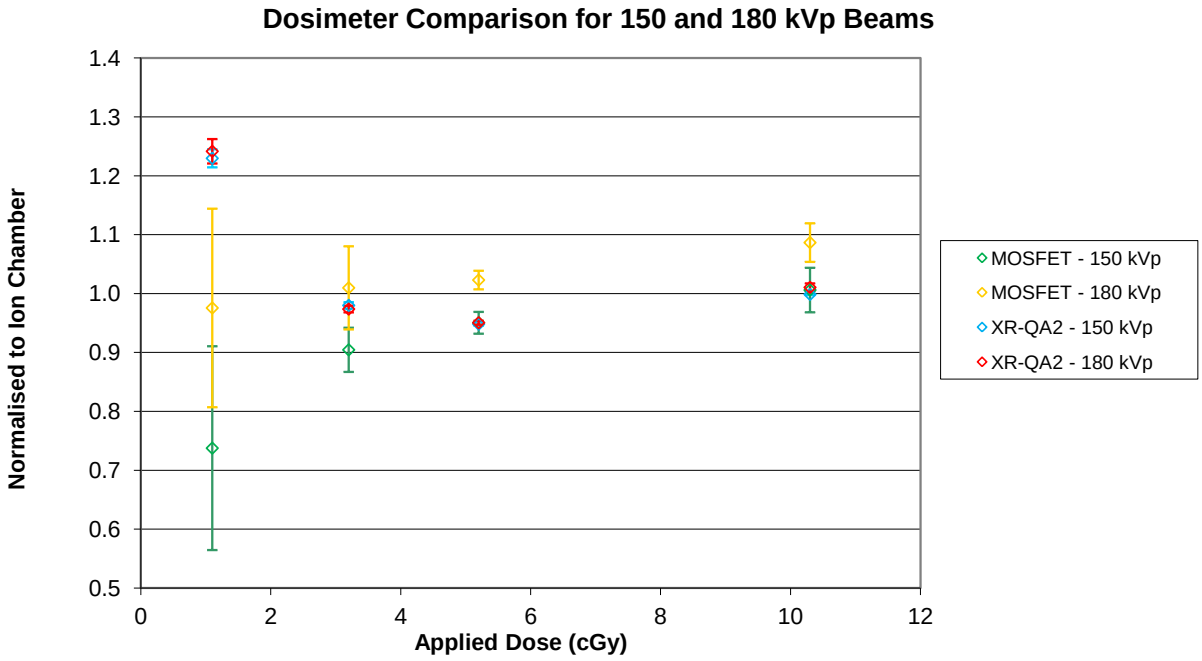

Figure 2.10: The comparison of XR-QA2 Gafchromic film and MOSFETs dosimeters for measurements made with 150 and 180 kVp orthovoltage beams. The measured doses were normalised to the applied doses, measured with a NE2571 graphite cylindrical ionisation chamber.

2.5 Concluding Remarks

In this chapter the suitability of TN-1002RD MOSFETs and Gafchromic film was investigated for measuring dose in the kV and MV range. MOSFETs are accurate dosimeters for measuring peripheral dose close to the irradiated field. At distances > 5 cm, the inaccuracy increases to 25%. The accuracy in MOSFET measurements within kV beams was found to be 10%. XR-QA2 is accurate to within 5% for measurements made within 150 and 180 kVp beams and exposures above 3 cGy. EBT2 Gafchromic film overestimates the dose by approximately 20% in the peripheral regions of MV beams. The reproducibility of MOSFETs for low dose deliveries was 26.6 and 50.4% in 150 and 180 kVp beams, respectively. In megavoltage beams, the reproducibility was 18.1%. Gafchromic film has good precision at low doses. The reproducibility of EBT2 for MV energy was 1.0%. For 150 and 180 kVp, the uncertainty of XR-QA2 film was 3.1 and 3.0%, respectively.

In the next chapter the relevant risk models are introduced to evaluate the risks associated with the doses measured using the above dosimeters.

Chapter 3

Risk Analysis

3.1 Introduction

Radiation induced second malignancies following radiotherapy are of concern, especially for younger patients who have a long life expectancy. Modern treatment techniques rely on image guidance to ensure the accurate targeting of tumour volumes and to minimise normal tissue toxicity[69–71]. Additionally, on-treatment imaging is used to observe inter- and intrafraction organ and tumour motion and may be performed as often as twice per fraction[72,73]. Although the dose from Cone-beam CT (CBCT) imaging is a fraction of that from planning CT, the dose is not insignificant when daily imaging is considered[2]. In this work, the risk of radiation-related cancer, due to radiotherapy and the necessary imaging, was assessed using an array of models; namely, the competition model[74] and the Biological Effects of Ionizing Radiation (BEIR) excess relative risk (ERR) and excess absolute risk (EAR) models, given in the BEIR VII phase II report[75].

3.2 Competition Model

The competition model takes into account the probability of inducing DNA mutations and the probability of the cells surviving irradiation. It is based on the linear quadratic equation and accounts for fractionated radiotherapy and can be expressed as:

$$Effect = \left(\alpha_1 D + \frac{\beta_1 D^2}{n}\right) \times exp\Big[- \left(\alpha_2 D + \frac{\beta_2 D^2}{n}\right)\Big] \tag{3.1}$$

where D is the total dose given in n fractions, α_1 and β_1 are radiation induced mutation parameters and α_2 and β_2 are cell survival parameters. The α/β ratios are assumed to be the same for the first (induction of DNA mutation) and second (cell survival) terms. α_1 values are rare in the literature, consequently approximations were made for this evaluation as suggested by Daşu *et al.*[74]. The quadratic terms in Equation 3.1 become insignificant at very low doses, resulting in an approximate linear relationship between dose and effect. Thus, the slope of the curve, α_1, is assumed to be equal to the risk coefficients found from epidemiological studies of populations irradiated with low doses[74]. These linear risk coefficients are obtained from ICRP[76].

The non-homogeneity of the dose distribution across the volume of concern is accounted for by calculating the risk in every dose interval of the dose-volume histogram, which is then summed to establish the total effect and follows as:

$$Total\ effect = \frac{\sum_i \Big(v_i \times Effect(D_i)\Big)}{\sum_i v_i} \tag{3.2}$$

Where v_i is the volume of tissue receiving dose D_i. In this work, the organ at risk volume was subdivided in the treatment planning system (TPS) such that the subvolumes centred around a measurement point. The dose measured using dosimeters on the surface of each subvolume was assumed to be the dose delivered to the whole subvolume. The competition model was used to determine the secondary cancer risk associated with dose in the periphery of the treatment fields and due to imaging.

3.3 Excess Relative Risk and Excess Absolute Risk Models

For comparison, additional models were used. The BEIR VII ERR and EAR models assume a linear relationship between dose and risk and are specific for low levels of ionising radiation (0 - 100 mGy). The excess absolute risk is the difference in incidence rates between the exposed and unexposed population and is the number of excess cases per 10,000 people per year. The relative risk (RR) is the ratio between incidence rates of the exposed and unexposed population and the excess relative risk is specified as, ERR = RR - 1. ERR and EAR are given by the same formula, however, the parameters are specific for each model:

$$ERR\ and\ EAR = \beta\ D\ exp[\gamma e^*]\left(\frac{\alpha}{60}\right)^{\eta} \tag{3.3}$$

where D is the dose (Sv); β is a sex specific risk coefficient which corresponds to the ERR/Sv and EAR/Sv at exposed age 30 and attained age 60 for ERR and EAR, respectively; α is the attained age (years); η is the exponent of attained age; γ is the per-decade increase in age at exposure over the range 0-30 years;

$$e^* = \begin{cases} (e-30)/10, & \text{if } e < 30 \\ 0, & \text{if } e \geq 30 \end{cases}$$

and e is the age of treatment (exposure);

The EAR and ERR risk models do not account for fractionation in treatment regimes and therefore, the benefits of the optimum therapeutic ratio between tumour control and late effects are unaccounted for. Despite this, these models were used to calculate the risk of radiation related cancer from dose exposures $\leq$ 1 Gy (e.g., from CT and CBCT scans) and the results were compared against the risks determined using the competition model.

3.4 Concluding remarks

In the absence of a single generally accepted model, several candidate models were used to calculate the approximate risk of radiation induced cancer. However, these models are not without limitations. The competition model, which factors in the probability of inducing DNA mutations and the probability of the cells surviving irradiation and accounts for fractionation in the dose delivery, is limited by the availability of specific model parameters, i.e., α_1. Furthermore, the competition model is designed to be used with dose volume histogram data from the treatment planning system to sum the effects of the dose per volume across the organ at risk, whereas, in this work, measured organ at risk doses to specified volumes were used. Fractionation is unaccounted for when using the EAR and ERR models, and consequently, the reduction in late site effects due to the improved therapeutic ratio is not considered. Nevertheless, for doses below 1 Gy, the ERR and EAR were calculated and compared with the competition model results.

The risk of radiation induced cancer was assessed for healthy tissue exposed to dose from CT, CBCT and concomitant dose from radiotherapy delivery.

Chapter 4

Case Study 1: Seminoma

4.1 Introduction

Testicular cancer is rare, having a global incidence of 0.8% of male cancers, with a slightly increased incidence in westernised countries (New Zealand 1.2%)[77]. It is the most common cancer in males of age 19-39 years in New Zealand[77] but remains one on the most curable cancers if treated in the early stages (5-year relapse-free rate of 95-97%)[78,79]. Almost all testicular cancer originate in the germ cells and are classified as either seminoma or non-seminoma cancers.

Testicular seminoma has a predictable disease progression, metastasising to the paraaortic lymph nodes[80]. For patients with a history of un-descended testes and/or abnormal nodal drainage, there is an increased risk of disease spread to the pelvic and ipsilateral common iliac lymph nodes[80]. Stage I seminoma is treated by orchidectomy followed by one of the following: surveillance, chemotherapy or radiotherapy to the paraaortic lymph nodes, including pelvic and iliac lymph nodes where appropriate. Lead shielding is routinely used to protect the remaining testis from radiation for patients undergoing radiotherapy inclusive of the pelvic and ipsilateral common iliac lymph nodes. Even though the testis is well removed from the paraaortic irradiation fields, scattered dose in the order of 1-6% of the prescribed dose has been measured[19,20]. The testicular dose was reduced to 0.4-3% when some form of gonadal shielding was fitted and consequently, the use of shielding is encouraged regardless of the

treatment field[19,20].

Since testicular seminoma occurs in a relatively young population, who after treatment have a long life expectancy, the risk of radiation induced cancer to the contralateral testis and the late side effect of infertility are of concern. A retrospective study assessing patients at least three years after treatment for testicular cancer found a 30% decrease in fertility. Treatment therapies included orchiectomy followed by either surveillance, radiotherapy and/or chemotherapy and radiotherapy was shown to have the greatest detrimental effect on fertility[18].

In this work the accumulative dose a patient receives while undergoing radiation treatment for testicular seminoma was measured to assess the risk of secondary cancer and late side effects. Dose contributions from CT, CBCT and treatment scatter were considered. Both paraaortic lymph node and extended field treatments were assessed with and without the lead shielding fitted.

4.2 Materials and Methods

A Varian iX linear accelerator (Varian Medical Systems, Palo Alto, CA) was used to deliver treatment to an anthropomorphic phantom. Radiation doses were measured with Gafchromic film and TN-1002RD MOSFET dosimeters and compared to the predicted dose of TPS. The treatment plans were created in Pinnacle^3 and computed using the collapsed cone convolution algorithm and a 4 mm dose grid. The potential risk of second testicular cancer due to radiotherapy treatment for seminoma was assessed using risk models (Chapter 3).

4.2.1 Treatment Planning Techniques

A Rando Phantom (Alderson Research Laboratories, Long Island City, New York) fitted with a wax scrotum (density = 0.9g/cm^3) moulded in the department workshop was positioned on the CT couch. Three surface measurement points were identified and marked with tape; one on the anterior, one on the posterior scrotal surface and one on the abdomen 5 cm superior

to the superior edge of the wax mould. These can be seen in Figure 4.1. Additionally, this tape prevented wax residue on the Gafchromic film. Lead gonadal clam-like shielding is used at treatment to protect the remaining testis, however, this results in image artefacts if fitted at CT imaging. To accommodate this, a replicate constructed from PVC is used. Both the pseudo and lead clam gonadal shielding were crafted in the department workshop. The phantom was scanned on a Siemens Somatom Sensation Open helical scanner (Siemens Medical Solutions, Erlangen, Germany) following departmental protocol for pelvis CT scans (120kV, 148 mA, 3 mm slice thickness). The scan extended from the T7/T8 joint to mid femur. The data set was exported for planning.

Figure 4.1: Rando positioned on the treatment couch with the posterior lead shielding fitted. MOSFETs are positioned at the abdominal and anterior scrotal measurement points demarcated by the green tape.

Two treatment plans consisting of an anterior/posterior parallel opposed beams were created using 18MV photons in Pinnacle^3 (Philips Medical Systems, Milpitas CA). The paraaortic (PA) plan consisted of a rectangular field 20 cm long and 8 cm wide to include the paraaortic lymph nodes with a prescribed dose of 20 Gy in 10 fractions. The kidneys were shielded by multileaf collimators (MLCs). This treatment was prescribed to 100% of the dose at the isocentre, which corresponds to the zero slice in the data set. The posterior beam (Gantry = 180°) was a mirror of the anterior beam (Gantry = 0°). The anterior beam digitally reconstructed radiograph, DRR, (Figure 4.2) shows the treatment field and kidney shielding. The second treatment plan, commonly referred to as a dogleg (DL), was

an extension of the PA to include the ipsilateral pelvic and common iliac lymph nodes with a prescribed dose of 30 Gy in 18 fractions. The prescription isocentre was positioned more inferiorly than in the paraaortic treatment plan and MLCs were used to shield the kidneys and the remaining testis (Figure 4.3). Again, the posterior beam was a mirror of the anterior treatment beam. The isodose distributions from the respective plans are shown in Figure 4.2, 4.3.

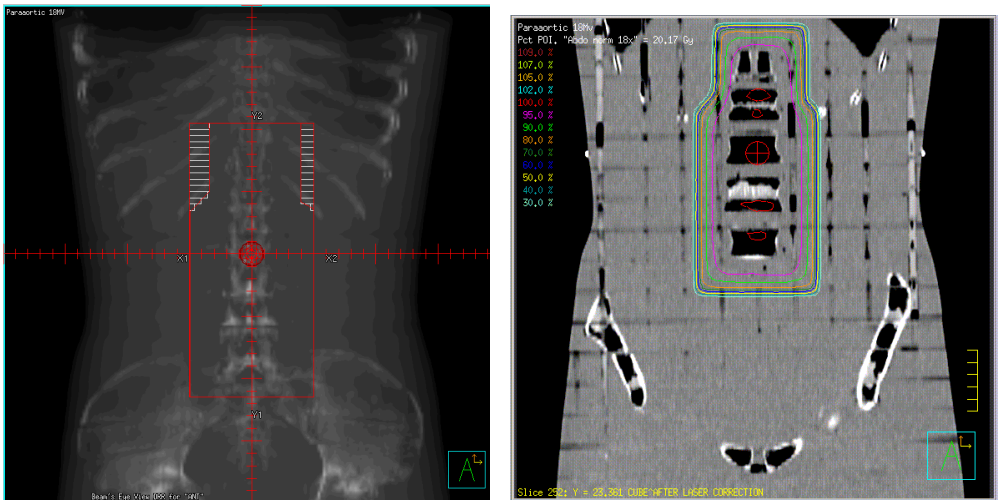

(a) A digitally reconstructed radiograph of the anterior treatment beam.

(b) A coronal view of the isodose distribution at the CT reference point.

Figure 4.2: The paraaortic treatment plan. (a) The centre of the beam is aligned with the isocentre (red wireframe sphere). (b) The pink and red isodose lines represent the 95% and 100% dose coverage, respectively.

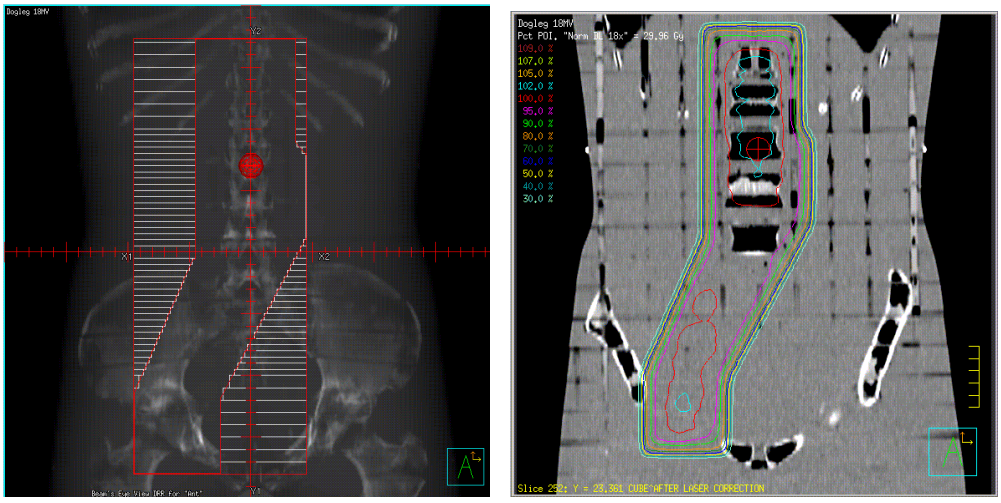

(a) A digitally reconstructed radiograph of anterior treatment beam.

(b) A coronal view of the isodose distribution at the CT reference point.

Figure 4.3: The Dogleg treatment plan. (a) The MLCs shielding the kidneys and testis can be seen in the DRR. (b) The turquoise, red and pink isodose lines represent the 102%, 100% and 95% dose coverage, respectively.

4.2.2 Measurements

CT

The Rando anthropomorphic phantom was positioned on the CT scanner bed and aligned with the lasers. A MOSFET was placed at the centre of the anterior and posterior scrotal and abdominal positions. The pseudo lead clam shielding was positioned to enclose the scrotum. Following departmental protocol, a topogram (scout scan) was carried out prior to a CT scan. The MOSFETs were read out within five minutes after each CT scan. The measurements were repeated three times with and three times without the clam shielding fitted. XR-QA2 Gafchromic film was positioned at the same locations and secured with tape, ensuring no more than 0.5 cm in from the film edge was covered. 1.5 x 3 cm^2 film strips were placed at the anterior and posterior scrotal positions and a 3 x 3 cm^2 piece of film was placed at the abdominal position. Using the same scanning technique, three CT scans were carried out with gonadal shielding and three without. An unexposed film piece was used for each scan. In keeping with calibration, the film was digitised 46 hours post irradiation and analysed as previously described.

CBCT

Rando was positioned on the treatment couch with the lead shielding in place and aligned with the lasers to the CT reference point. The half bow tie was fitted and a pelvis CBCT image, using the standard imaging protocol (125 kVp, 706 mA s, 360°), was taken for pre-treatment image matching. The CBCT field was 16 cm wide, inclusive of the abdominal measurement point, however, the scrotum lay out of the imaging field. Three CBCT images were performed with XR-QA2 film in place and three with MOSFET dosimeters. These were repeated without the shielding fitted.

Treatment

EBT2 Gafchromic film was cut to size, 3 x 1.5 cm^2 for the scrotal measurement points and 3 x 3 cm^2 for the abdominal point and secured in place using tape. The orientation of the film

was kept consistent and care was taken to ensure that no more than 0.5 cm in from the film edge was covered with tape. Rando was set up on the treatment couch, with the gonadal shielding fitted, using localisation lasers to match the position at CT. One fraction of the paraaortic treatment was delivered. A total of three measurements with shielding and three without shielding were performed. These measurements were repeated with MOSFETs. Measurements were carried out in the same manner for the dogleg treatment plan, using both MOSFET and film dosimeters.

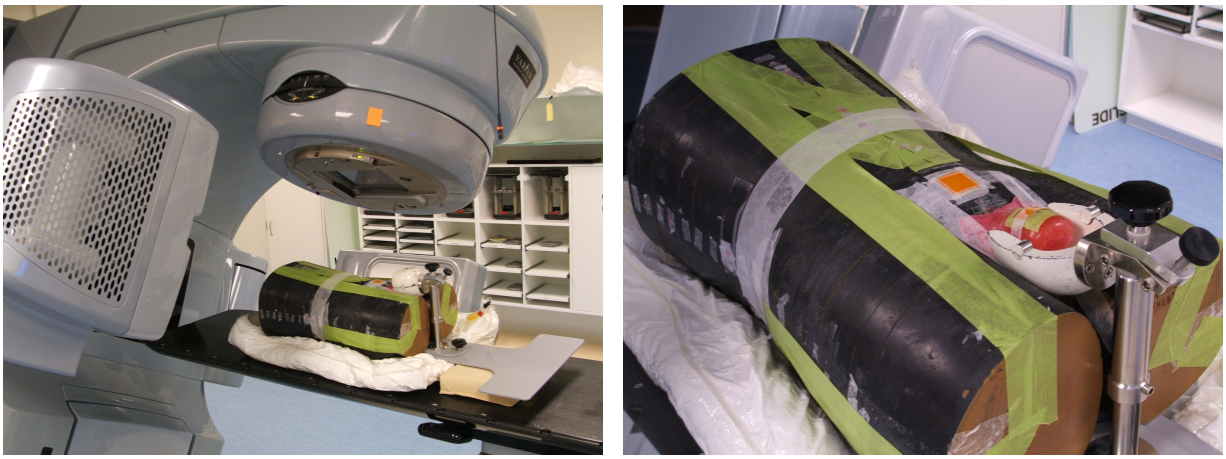

(a) Full lead shielding fitted. (b) Gafchromic film placement.

Figure 4.4: (a) Rando set up on the treatment couch with EBT2 film positioned at the measurement points. The treatment gantry angle is not shown.(b) Half the clam shielding is removed showing the placement of the film dosimeter. (The posterior scrotal measurement point is not seen.)

4.2.3 Pinnacle^3 Dose

The PVC shielding was contoured in the TPS and the density was overridden to that of lead (11.3 g/cm^3). Points of interest (POIs) were created at the three respective measurement points, directly below the external contour for comparison with doses measured with Gafchromic film. MOSFET dosimeters have an inherent build up of 1 mm due to the epoxy bulb. In order to compensate for this, additional POIs were created at a depth of 1 mm below the first set of points. The dose was recorded at each POI and at five surrounding points located 2 mm inferior, superior, posterior and lateral (two points) of the POI, respectively. The dose was not recorded anteriorly as this was in air. The mean of the six point doses was compared to the measured doses made with shielding fitted.

4.2.4 Risk Analysis

The competition, BEIR VII ERR and EAR models were used to assess the risk of radiation induced cancer in the remaining testis as a result of the accumulative dose received throughout the treatment process. These models have been previously described (Chapter 3). The mean of the anterior and posterior testicular dose was employed in all models for risk assessment.

An α/β ratio of 12-13 Gy[81,82] for early responding normal testis tissue was used for the competition model. The nominal risk co-efficient, α_1 = 2x10^{-3} Gy^{-1} and α_2 = 0.25 Gy^{-1} are assumed, resulting in β_1 and β_2 values of 1.67x10^{-4} and 2.08x10^{-2}, respectively[74,76].

For the BEIR VII model, no specific risk model parameters are given for estimating cancer incidence from dose to the testis. As such, the risk model parameters for all solid cancers, which excludes thyroid and nonmelanoma skin cancers, were used. For the given ERR parameters, β = 0.33 (0.24, 0.47 95% CI), γ = -0.30 and η = -1.4, and dose, D, the testicular cancer risk is given by;

$$ERR = D\ 0.33\ \exp[-0.3e^*]\left(\frac{\alpha}{60}\right)^{-1.4}$$

The EAR model, with parameters β = 22 (15, 30 95% CI), γ = -0.41 and η = 2.8, results in an estimate of the additional cancer incidence per 10,000 people per year and is given as follows:

$$EAR = D\ 22\ \exp[-0.41e^*]\left(\frac{\alpha}{60}\right)^{2.8}$$

where,

$$e^* = \begin{cases} (e-30)/10, & \text{if } e < 30 \\ 0, & \text{if } e \geq 30 \end{cases}$$

α is the attained age, and

e is the age at treatment (exposure).

These models were evaluated for exposed ages, $e = 25$ and 35 y and attained ages 20 years later; $\alpha = 45$ and 55 y.

The risk of radiation induced cancer due to CBCT was assessed for two common imaging schemes: daily (n=18) and imaging the first three days followed by weekly CBCT (n=6). The CT associated risk was calculated assuming only one CT was performed.

4.3 Results

4.3.1 CT & CBCT Imaging

The mean (95% CI) of the measurements recorded while acquiring images is given in Table 4.1. For CBCT imaging using XR-QA2, a dose reduction to the testis of more than 50% is seen when the lead shielding is fitted. In contrast, the anterior and posterior MOSFET measurements were 0.01 and 0.13 cGy with shielding and 0.03 and 0.09 cGy without, showing little variation between those with and without shielding present and falling within the 95% CI. The dosimeters were positioned at least 5 cm from the inferior edge of the imaging field, resulting in a low particle flux to this point. Furthermore, the signal is attenuated by the lead shielding and the epoxy bulb, for MOSFETs. The dosimeter results from CT acquisition are in good agreement. With the pseudo shielding fitted, the dose to the testis is reduced by approximately 50%.

4.3.2 Treatment Delivery

The mean (95% CI) of the dose measurements acquired for DL and PA treatment deliveries are given in Table 4.2. In general, less dose was recorded for the paraaortic treatment. This was expected as the DL fields were closer to the measurement points. MOSFET and EBT2 film measurements were in good agreement at the abdomen for all treatment scenarios. At the anterior scrotum, a dose reduction of approximately 1/4 was seen with the gonadal shielding fitted when measuring with EBT2 film. Contrary to this, little change was recorded at the posterior scrotal position when the shielding was fitted. The MOSFET measurements

Table 4.1: The results displayed are for a single scan of each imaging technique. Measurements were made with and without gonadal shielding present.

Imaging Dose (cGy)					
Dosimeter	Technique	Shielding	Regions of Interest		
			Abdomen	ANT	POST
MOSFET	CBCT	Y	2.19 ± 0.76	0.01 ± 0.03	0.13 ± 0.26
		N	3.09 ± 0.23	0.03 ± 0.05	0.09 ± 0.18
	CT	Y	2.38 ± 0.27	1.36 ± 0.24	1.17 ± 0.15
		N	2.60 ± 0.42	2.40 ± 0.67	2.71 ± 0.25
XR-QA2	CBCT	Y	3.25 ± 0.03	0.19 ± 0.01	0.02 ± 0.01
		N[1]	3.26 ± 0.02	0.49 ± 0.01	0.46 ± < 0.01
	CT	Y	2.63 ± 0.12	1.70 ± 0.04	1.26 ± 0.05
		N	2.56 ± 0.18	2.28 ± 0.17	2.35 ± 0.05

[1] The mean of two measurement sets. The third set was discarded due to visible anomalies.

at the testicle are a fraction of the film results ($< 1/3$). This is due to the low particle flux at these positions, which is attenuated further by the epoxy bulb and the lead shielding.

The mean (95% CI) of the point dose measurements predicted in the treatment planning system are given in Table 4.3. The TPS predicted doses to the testis are approximately 1/3 of those measured with Gafchromic film for DL treatment fields. For this plan delivery, the MOSFET results were in better agreement with the TPS, however, they in themselves had large uncertainties. Overall, there was little agreement with the measured results.

Table 4.2: Dose measurements were recorded with and without lead shielding fitted for paraaortic and dogleg treatment techniques.

Seminoma Treatment Dose (Gy)					
Dosimeter	Technique	Shielding	Regions of Interest		
			Abdomen	ANT	POST
MOSFET	Dogleg	Y	1.34 ± 0.28	0.18 ± 0.19	0.08 ± 0.06
		N	1.23 ± 0.40	0.26 ± 0.31	0.06 ± 0.07
	PA	Y	0.49 ± 0.11	0.08 ± 0.11	0.00 ± 0.00
		N	0.50 ± 0.18	0.00 ± 0.00	0.03 ± 0.12
EBT2	Dogleg	Y	1.72 ± 0.06	0.63 ± 0.02	0.59 ± 0.10
		N	1.77 ± 0.02	0.83 ± 0.17	0.53 ± 0.28
	PA	Y	0.70 ± 0.07	0.32 ± 0.04	0.27 ± 0.06
		N	0.68 ± 0.11	0.43 ± 0.02	0.19 ± 0.02

Table 4.3: Seminoma point doses in the TPS.

TPS Point Dose (Gy)				
	Point Depth	Abdomen	Anterior	Posterior
Dogleg	Surface	1.53 ± 0.12	0.19 ± 0.01	0.16 ± 0.01
	1 mm	1.74 ± 0.08	0.19 ± 0.01	0.16 ± 0.01
PA	Surface	0.14 ± 0.01	0.00 ± 0.00	0.00 ± 0.00
	1 mm	0.15 ± 0.01	0.00 ± 0.00	0.00 ± 0.00

4.3.3 Risk Analysis

The risk of radiation induced testicular cancer was assessed for concomitant doses received while undergoing radiotherapy for testicular seminoma (Table 4.4). The mean of the anterior and posterior scrotal doses over the course of treatment was evaluated. As a conservative approach, the maximum dose was used to assess risk (i.e., Gafchromic film results). ERR and EAR models were used to calculate the risk of cancer 20 years after the initial treatment, assuming first treatment at either 25 or 35 years of age. The risk of radiation induced cancer decreases with increasing age of first treatment. The accumulative risk, which combines the risk associated with treatment and imaging, was calculated for the ERR and EAR models, assuming treatment at 25 years of age. In summary, the EAR model estimates an additional 7.4 and 8.3 cancers per 10,000 people per year treated for seminoma with dogleg fields, with and without shielding, respectively. This estimate was 3.6 and 3.9 for paraaortic fields. The risk of radiotherapy treatment for seminoma inducing cancer in the remaining testis is 0.4% and 0.2% for dogleg and paraaortic treatments irrespective of gonadal shielding.

Table 4.4: Risk estimates of radiation induced testicle cancer based on the ERR, EAR and competition risk models. EAR and ERR were calculated at 20 years post treatment for age at treatment of 25 or 35 years (e = 25, 35y and α = 45, 55y). The results are given as 25y / 35y. The accumulative risk from CT, daily CBCT and treatment was considered at treatment age of 25y.

Testicular Cancer Risk Estimates				
Risk Model	Radiation Source		Shielding	No Shielding
Competition Model	Dogleg		0.10%	0.12%
	Paraaortic		0.06%	0.06%
	CBCT	*n = 6*	0.001%	0.006%
		n = 18	0.004%	0.017%
	CT		0.003%	0.005%
ERR	Dogleg		0.35% / 0.17%	0.39% / 0.19%
	Paraaortic		0.17% / 0.08%	0.18% / 0.09%
	CBCT	*n = 6*	0.004% / 0.002%	0.016% / 0.008%
		n = 18	0.011% / 0.005%	0.049% / 0.023%
	CT		0.008% / 0.004%	0.013% / 0.006%
EAR	Dogleg		7.36 / 6.98	8.21 / 7.78
	Paraaortic		3.56 / 3.37	3.74 / 3.55
	CBCT	*n = 6*	0.08 / 0.08	0.34 / 0.32
		n = 18	0.23 / 0.22	1.02 / 0.97
	CT		0.18 / 0.17	0.28 / 0.27
Accumulative Risk $_{e\,=\,25y}$	Dogleg[1]		0.35%	0.39%
	Paraaortic[1]		0.17%	0.19%
	Dogleg[2]		7.37	8.28
	Paraaortic[2]		3.57	3.89

[1] ERR model.
[2] EAR model. Value expressed in cases per 10,000 people per year.

4.4 Discussion

For a total prescription of 20.0 Gy to the paraaortic region, the mean dose measured using film to the contralateral testis was 0.30 ± 0.08 Gy and 0.31 ± 0.04 Gy with and without lead shielding, respectively. For the PA region, including the pelvic and ipsilateral common iliac lymph nodes, and with a prescribed dose of 30.0 Gy, the mean testicular dose was 0.61 ± 0.11 Gy and 0.68 ± 0.39 Gy with and without shielding, respectively. Dose reductions up to 10% were observed with shielding fitted at treatment. This increased to approximately 25% when considering the anterior scrotal dose alone. These doses are approximately two times the doses previously reported. Bieri *et al.*[19] measured mean doses, using TLDs, of 0.09 Gy (± 0.05 SD) and 0.26 Gy (± 0.12 SD) with and without gonadal shielding, respectively, for a prescribed dose of 25.2 Gy to the PA region. For the same dose prescribed, only with dogleg treatment fields, mean doses of 0.55 Gy (± 0.20 SD) and 0.21 Gy (± 0.07 SD) were measured, without and with shielding, respectively. Similarly, Jacobsen *et al.*[83] reported a mean dose of 0.32 Gy (± 0.08 SD) to the shielded testis for a delivered dose of 30.0 Gy with dogleg fields. The contralateral testicle was shielded using a 5 mm lead belt and a 5 cm thick lead block. The disparity between the doses in this work and those reported may be due to differences in shielding techniques used and variations in the type and placement of dosimeters.

Dose reductions to the remaining testis of up to 36% and 78% were recorded with gonadal shielding fitted at CT and CBCT acquisition respectively.

Despite the relatively large scatter dose from treatment, the accumulative risk of radiation induced cancer to the remaining testis when treating early stage seminoma, with or without shielding fitted, was found to be 0.4% and 0.2% for dogleg and paraaortic treatment fields. An additional 7.4 and 8.3 cancers per 10,000 people per year were estimated as a results of radiotherapy treatment for seminoma with dogleg fields, with and without shielding, respectively. These estimates were 3.6 and 3.9 for paraaortic fields. The risk was found to decrease with increasing age at diagnosis. Although the risk is low, a greater incidence of secondary cancers has been reported[16,17,84,85]. A multicentre investigation involving 839 patients treated with either radiotherapy (758), chemotherapy (76) or surveillance (5) as-

sessed the significance of second malignancies following treatment for seminoma. Twenty two second cancers were found, 13 of which were contralateral testicular tumours[16]. That is to say, 1.6% of patients developed a testicular second cancer. The median follow-up was 3.9 years. A similar investigation involving 116 patients treated with orchidectomy followed by radiotherapy revealed 3 subsequent testicular cancers (2.6% of patients)[17]. The observed testicular cancer incidence was twice the expected incidence. A third study, with follow-up periods ranging 5-29 years, observed only 1 (0.8%) second testicular cancer from 128 patients treated for early stage seminoma[84].

The cancer risk associated with diagnostic imaging was found to be less than 0.05%. The increased risk related to performing daily (18) verses six CBCTs is negligible. The reported role of diagnostic imaging in cancer induction is conflicted in the literature. van Walraven *et al.*[86] concluded that the excess risk of second cancers among testicular cancer survivors is not associated with diagnostic imaging. This population-based study observed the incidence of second malignancies in 2,569 men who were treated with either surveillance or chemotherapy for testicular cancer and received 10 CT scans in 5 years after diagnosis. The median follow-up was 11.2 years. In contrast, a model based study report a lifetime cancer risk ranging from 1 in 39 to 1 in 85 for a similar surveillance protocol[87]. Nevertheless, the majority of diagnostic imaging in this work was CBCT imaging, which based on this work delivered doses approximately 1/5 of those recorded at CT acquisition.

Radiation is not the only contributing factor to secondary cancers as patients who receive orchiectomy alone for the treatment of testicular cancer are at increased risk of second cancers compared to the general population[10]. Nevertheless, the dose to the remaining testis should be keep as low as reasonably achievable (ALARA)[76], not only to reduce the risk of second malignancies, but of alternative long term side effects as well. Testicular doses of 0.2-0.7 Gy result in a temporary reduction in sperm count, returning to normal within 12-24 months[88]. While doses above 1.2 Gy indicate permanent testicular damage[89].

The risk models used are not without limitations. There was insufficient data to derive EAR and ERR models for testicular cancer. As such, model parameters for all solid cancers were used as a best estimate. The competition model[74] requires α_1 values which are not

widely available; ICRP nominal risk coefficients were used as an alternative. Moreover, the competition model is designed to be used with dose volume histogram data to sum the effects of the dose per volume across the organ at risk. While in this instance, the mean dose to the whole testicular volume was analysed.

In summary, the risk of radiation induced testicular malignancies is minimal for doses received while undergoing radiotherapy for seminoma cancer. Still, gonadal shielding should be fitted to limit unnecessary dose to the testis, thereby reducing radiation-related infertility and second cancers, regardless of the treatment fields.

4.5 Conclusion

Mean testicular doses of 0.30 ± 0.08 Gy and 0.31 ± 0.04 Gy with and without lead shielding, respectively, were measured for a prescription of 20 Gy to the paraaortic region. Seminoma radiotherapy via dogleg fields resulted in respective mean doses of 0.61 ± 0.11 Gy and 0.68 ± 0.39 Gy, with and without shielding. The dose to the remaining testis was reduced when shielding was employed at treatment (10%), planning CT imaging (36%) and pre-treatment CBCT imaging (78%). The risk of radiation induced second cancers associated with the accumulative dose from treatment and imaging is low; 0.35% and 0.17% for dogleg and paraaortic treatment fields with shielding and 0.39% and 0.19% without shielding, respectively.

Although radiation is not the only contributing factor to secondary cancers, the dose to the testis should be limited to minimise this risk and other long term complications, such as infertility. This can be achieved by using appropriate gonadal shielding, irrespective of the treatment fields employed.

Chapter 5

Case Study 2: Breast Cancer

5.1 Introduction

Breast cancer is the most common female cancer in the world, accounting for 22.9% of all incidences. It is most commonly found in postmenopausal woman, but can occur at any age[77]. The treatment prescribed depends on the type of disease and clinical staging in accordance with the International Union Against Cancer (UICC) Tumour, Nodes and Metastases (TNM) classification. Radiotherapy following surgery reduces the risk of recurrence at five years post treatment from 26% to 7%[90] and aids local disease control[90–92]. As such, breast conserving surgery or mastectomy with adjuvant radiotherapy to the whole breast or chest wall, respectively, is the standard care path, followed by chemotherapy and/or endocrine therapies as required. For over several decades breast cancer has been treated with tangential fields, limiting unnecessary dose to the heart and lungs. Dose uniformity is aided by physical wedges, which were later superseded by dynamic wedges. Currently, more conformal techniques, such as forward planned IMRT, have been adopted as the standard in planning breast volume tangential irradiation. The prognosis of breast cancer is good if treated in the early stages of the disease, with a 5 year relative survival rate of 98.4%. This decreases to 83.9% for regional disease at diagnosis[93]. However, the risk of radiation induced cancer and late side effects, such as cardiac toxicity and pneumonitis, remain[94]. Although the radiation treatment is conformal to the diseased breast, healthy tissue will receive dose from internal

radiation scatter, collimator scatter and radiation leakage through the head of the treatment machine. Additionally, the normal tissue will receive dose contributions from planning CT and pretreatment imaging. The lungs[95,96], heart[96–98] and contralateral breast[21,22] are the surrounding organs most commonly assessed in breast cancer radiotherapy and the dose received is well known. The dose to the thyroid from early stage breast cancer radiotherapy is rarely measured as it lies away from the treatment field, however, hypothyroidism after loco-regional breast cancer radiotherapy has been seen although the link between the two is debated[99,100]. Based on a retrospective cohort study, Huang *et al.* showed that the risk of radiation-associated thyroid carcinoma following radiotherapy for breast carcinoma is undectectable[101]. Although the contralateral breast dose from therapy and imaging for breast carcinoma has been assessed independently, to the author's knowledge, the total combined dose to the radiosensitive contralateral breast and thyroid has not been evaluated to date. In this work, dose contributions from imaging modalities, CT and cone-beam CT (CBCT), and treatment were measured and the risk of radiation induced cancer assessed.

5.2 Materials and Methods

The dose to the contralateral breast and thyroid was measured on an anthropomorphic phantom using Gafchromic film and TN-1002RD MOSFET dosimeters and compared to that predicted by the TPS. Treatment was planned using Pinnacle^3 (collapsed cone convolution algorithm and 4 mm dose grid) and delivered on a Varian iX linear accelerator (Varian Medical Systems, Palo Alto, CA) equipped with On-Board Imager® (v1.4) and having CBCT capability. Risk models (Chapter 3) were used to calculate the possible risk of second cancers due to breast radiotherapy.

5.2.1 Treatment Planning Techniques

The contralateral breast dose has been studied by many authors using humanoid phantoms fitted with commercial breast moulds (see e.g. RANDO® Phantoms, The Alderson Radiation Therapy Phantom), though these do not accurately represent the typical breast tissue

distribution of a patient on the treatment couch. To overcome this, a human model was used to create wax breast moulds to fit an anthropomorphic phantom, Rando, replicating the typical patient of cup size C and breast separation 22 cm. These moulds were separate and fixed with tape for each use as required. All future references to Rando assume the breast moulds were fitted unless stated otherwise. Eight measurement points were identified on the surface of the contralateral breast, marked with tape and the centre crossed with pen: three at each of 2.5 cm and 12 cm from midline, at displacements of 5, 10 and 15 cm from the superior border, respectively and two on the lateral edge of the breast at 10 and 15 cm from the superior field edge, keeping in line with the other measurement points. The points identified are shown in Figure 5.1. One measurement point was selected at the position of the thyroid on the surface of the phantom. External fiducial markers were affixed in order to locate the measurement points on the CT scan. Rando was positioned supine on a MEDTEC Breastboard (elevation notch 4, head rest 1, notch 3), scanned on a Siemens Somatom Sensation Open CT Scanner as per departmental protocol (120 kV, 96 mA, 3 mm slice thickness) and the data set was exported to Pinnacle[3] for planning.

Figure 5.1: Rando positioned on the breast board with the wax breast moulds fitted. MOSFETs are positioned on the nine measurement points; eight on the contralateral breast (green squares) and one at the position of the thyroid.

The right breast volume was delineated, keeping within 0.5 cm of the external and ipsilateral lung contours. In order to compare the dose from different treatment techniques and energy modalities, five breast plans were created, namely, 6MV and 10MV Step and Shoot

(S&S), 6MV and 10MV Enhanced Dynamic Wedge (EDW) and 6MV physical wedge (PW). Planning with physical wedges using a 10MV beam was not commissioned in our department. All plans were designed by the author following departmental protocol and consisted of parallel opposed isocentric tangential fields treating the right breast with a prescribed dose of 45 Gy in 25 fractions. An open field 12 cm wide and 25 cm long was used across all beams and plans. The anterior edge of the field extended 2 cm beyond the breast tissue to compensate for breathing motion. The field length extended inferiorly from the suprasternal notch to 2 cm below the breast. Due to the necessary length of the field, a half beam block arrangement was used in all plans except PW. The X-jaws have a maximum traverse of 10 cm when an external wedge is fitted, thus both X-jaws were open to produce the desired volume coverage. The superior and posterior beam edges were matched using Casebow principles[102] resulting in couch angulations 3° and 357° for lateral and medial tangent beams, respectively. The weighting of the medial and lateral beams was almost equivalent in each treatment plan.

The contralateral breast volume was contoured to mimic the treatment volume and further subdivided into eight regions (see Figure 5.2b), each orientated around a fiducial marker. The three medial regions were identified sub-volumes 1-3, with one being the most superior. Sub-volumes 4-6 represent the middle three regions and 7 and 8 the lateral regions, with eight being the inferior region. The volume of each sub-volume, extracted from the treatment planning system, is given in Table 5.1. The thyroid was delineated with a resulting volume of 3.9 cm^3.

Table 5.1: The volumes of the contralateral breast sub-regions.

Contralateral Breast Sub-volumes								
Region	1	2	3	4	5	6	7	8
Volume (cm^3)	101.1	152.0	131.4	123.5	271.9	183.4	212.2	117.3

Physical wedge pair planning

6MV photons were prescribed in four fields, two medial and two laterals, to achieve the desired 95% coverage of the target volume. Approximately 90% of the dose was delivered

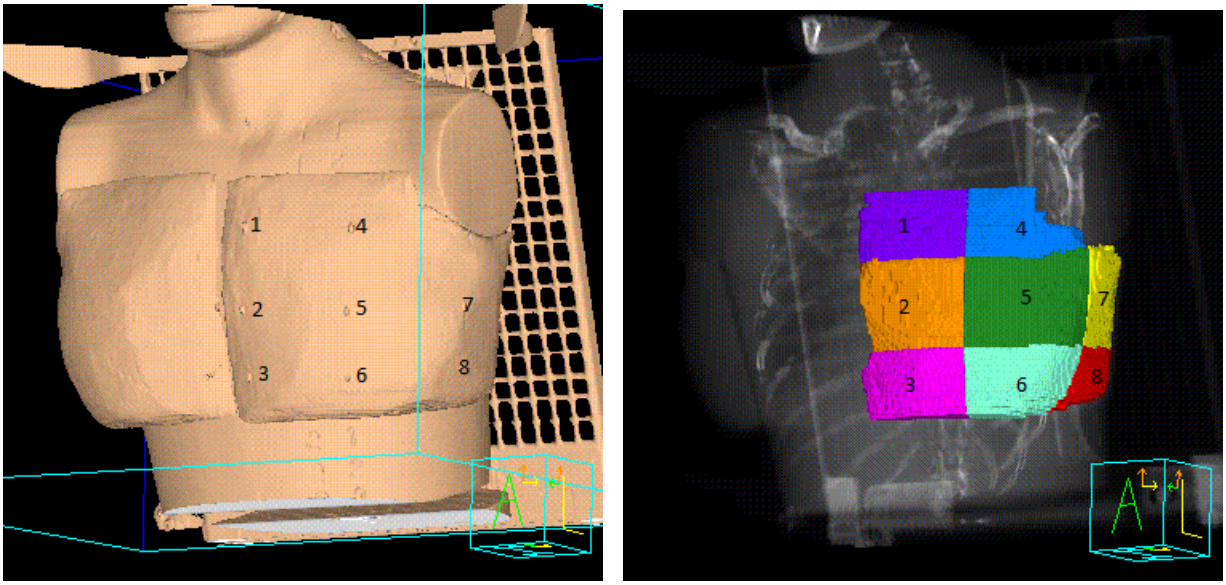

(a) Skin surface render of the breast phantom.

(b) DRR depicting the sub-volumes.

Figure 5.2: An illustration of the breast volume sub-divided in comparison with the skin surface.

through 15° wedged beams. The remaining dose was delivered through segmented fields which were added to shield hotspots and reduce the dose gradient across the volume. These fields used Multileaf Collimation (MLCs) to block areas of high dose and delivered a minimum of 10 Monitor Units (MU).

Enhanced dynamic wedge pair planning

The EDW technique simulates a physical wedge by moving one of the Y-jaw collimators from an open field to within 0.5 cm of the opposing jaw. The dose rate and speed at which the jaw moves vary to imitate assorted wedge angles. This technique reduces the time the patient is on the couch as radiation therapists do not need to enter the room to physically change wedges and results in less dose to the contralateral breast[103,104]. EDWs of 15° and 10° were prescribed on the medial and lateral tangents when planning with a 6MV beam while 10° for both 10MV fields. Additional unwedged segments were added to reduce hotspots in both plans with a minimum deliverance of 10MU. The collimator was rotated to 90° to facilitate this treatment technique.

Step and Shoot IMRT planning

For this forward planned treatment technique MLC fields (commonly known as control points) are added to improve the homogeneity of the dose distribution across the treatment volume. MLCs are shaped to isodoses of the relevant open field beam to shield areas of excessively high dose. A maximum of four control points were used. Each control point delivered a minimum of 5MU with at least 80% of the total beam dose delivered through the open field, as per departmental protocol. S&S plans were created using both 6 and 10MV beams.

Figure 5.3 displays the resulting isodose distributions at the zero slice (CT reference) for the five treatment plans developed. The pink and red isodose lines represent the 95 and 100% dose coverage, respectively.

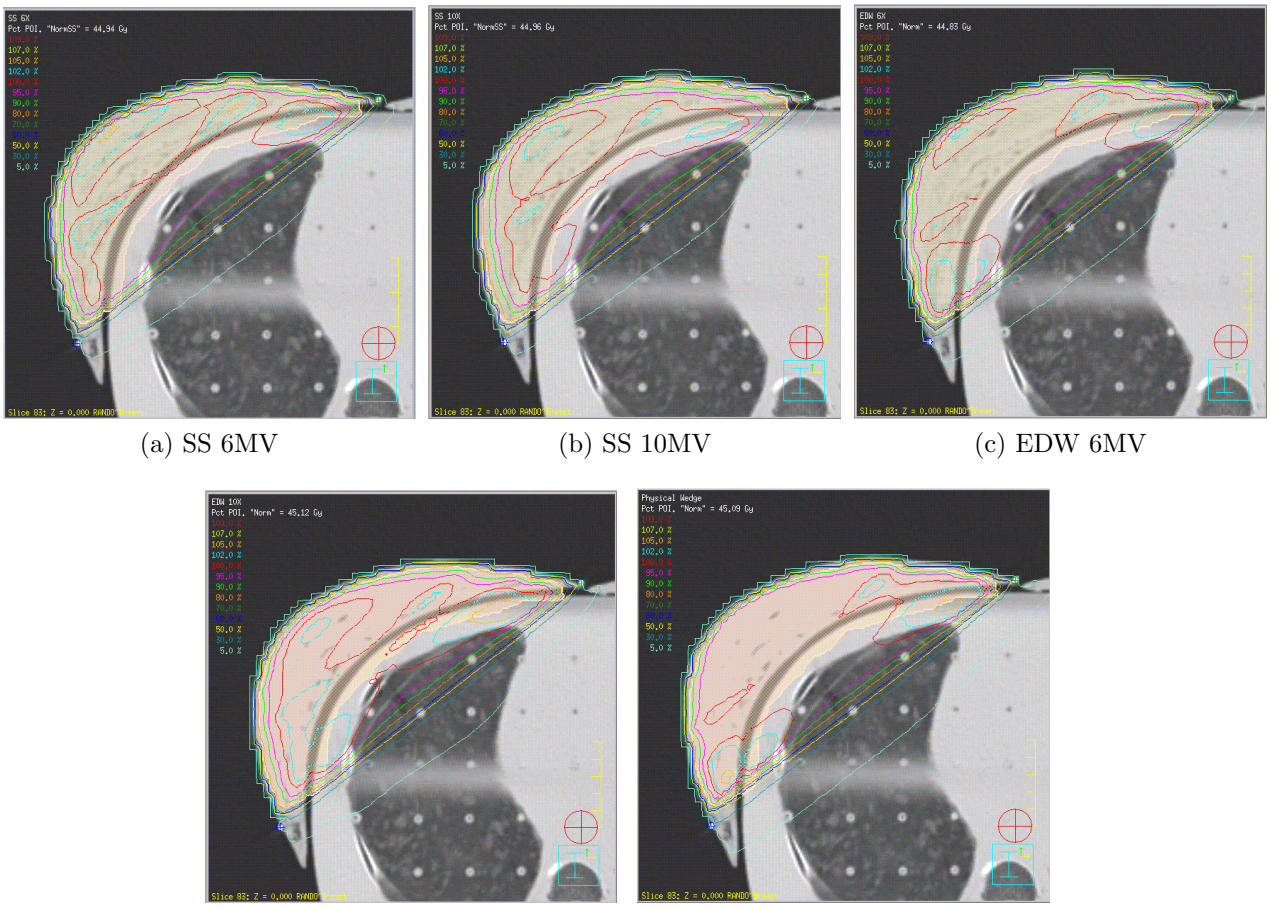

(a) SS 6MV (b) SS 10MV (c) EDW 6MV

(d) EDW 10MV (e) PW 6MV

Figure 5.3: Isodose distribution on the zero slice (CT reference) for the five breast plans. The pink and red isodose lines represent the 95 and 100% dose coverage, respectively.

5.2.2 Measurements

Planning CT

Rando was positioned on the CT scanner bed using the established breast board and head rest settings and aligned with the in-room lasers. Eight MOSFETs were placed centrally at the predetermined positions on the surface of the contralateral breast and secured with tape. One MOSFET was taped at the level of the thyroid on the 'skin' surface. A lateral topogram was carried out followed by a CT scan as per departmental protocol, extending from the lower mandible to the mid-abdomen. The MOSFETs were read out within five minutes following the CT scan. Two repeat measurements were taken, allowing at least five minutes between consecutive CT scans. 3 x 3 cm^2 XR-QA2 Gafchromic film squares were taped at the same locations, with a 4 x 4 cm^2 square positioned between phantom slices at the level of the thyroid. All film pieces were marked to ensure the original orientation was maintained. The tape did not encroach more than 0.5 cm when securing the film edges. The same scanning technique was used and a total of three measurements were performed. The film was scanned 46 hours post irradiation and analysed as previously described with the exception of the thyroid measurement films, for which the mean dose to a horseshoe-like area mimicking the thyroid was evaluated. The area, shown in Figure 5.4, is 3 cm along the x- and y-axis.

Cone-Beam Computed Tomography

Rando was positioned on the treatment couch and aligned with the lasers at the CT reference. Of the three couch shifts to the treatment isocentre, only the superior shift could be carried out, thus preventing couch collisions with the CBCT 360° gantry arc. However, this is not a method of best practice as applying couch shifts after imaging to ensure accurate patient positioning can introduce treatment errors. With the half bowtie filter fitted Low-dose thorax CBCT images, using the standard imaging protocol (110 kVp, 20mA, 20ms), were acquired; three with MOSFETs and three with XR-QA2 Gafchromic film positioned as previously described (section 5.2.2). The field length was 16 cm and encompassed sub-volumes 1, 2, 4, 5 and 7.

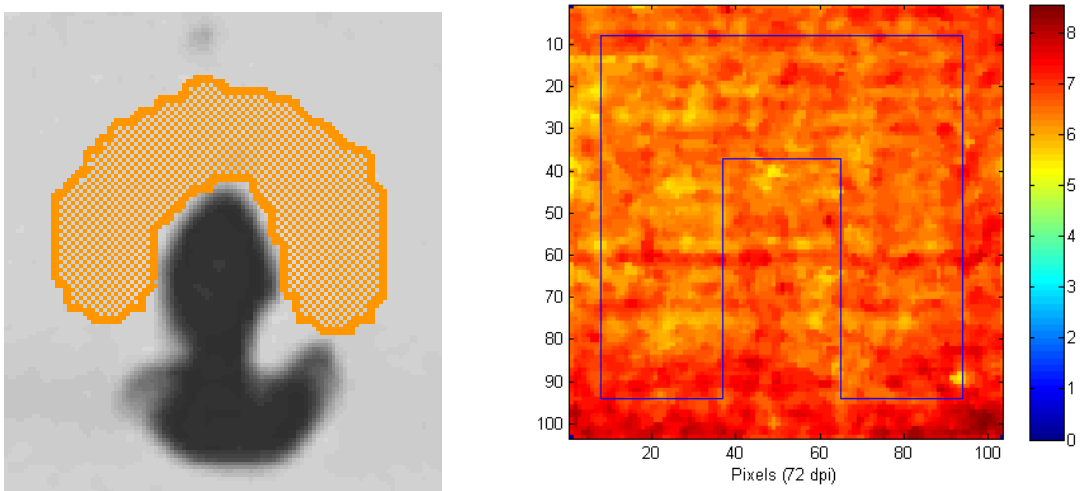

(a) Delineated thyroid contour in the TPS.

(b) Area of film used for analysis.

Figure 5.4: The horseshoe-like area used for film analysis of the thyroid measurements. The shape is comparable with the delineated thyroid in the TPS.

Treatment

Following CBCT, the remaining lateral and vertical shifts to the treatment isocentre were made. The dose to the contralateral breast and thyroid from a single fraction of each treatment technique was measured, first with EBT2 Gafchromic film. The film size and placement was consistent with previous measurements. A total of three measurements were made for each treatment technique. This was repeated using MOSFET dosimeters. The MOSFET readings were recorded after each fraction and the film was digitised 1 day later, keeping in agreement with the MV film calibration.

5.2.3 Pinnacle^3 Dose

In the TPS, the density of the metal fiducial markers was overridden to 0 g/cm^3 to avoid interference with the dose distribution at the surface of the phantom. Points of interest (POIs) were created directly below the reference fidicial markers on the contralateral breast and at the level of the thyroid for comparison with dose measured using Gafchromic film. For comparison with MOSFET dosimeters, POIs were created 1 mm below the first set of points to compensate for the inherent build of the MOSFETs due to the epoxy layer. The dose was recorded at each POI and at five surrounding points located 2 mm inferior, superior, posterior

and lateral (two points) of the POI, respectively. The dose was not recorded anteriorly as this point was in air. For each treatment plan, the mean of the six point doses was compared to the measured doses. Additionally, the mean dose to the thyroid volume was extracted from the TPS dose volume histogram (DVH) data.

5.2.4 Risk Analysis

The risk of radiation induced cancer in the thyroid and contralateral breast were assessed using an array of models previously described (Chapter 3). The competition risk model was employed for doses from both treatment and imaging, while the ERR and EAR models were used to assess only CT and CBCT doses. For the competition model, an α/β ratio of 3.4 Gy (2.3, 4.5 95% CI) was used to assess late effects of normal breast tissue[105,106] and a generalised α/β ratio for late responding tissue of 3 Gy was assumed for the thyroid. The risk coefficients, $\alpha_{1\ breast} = 0.011$ Gy^{-1}, $\alpha_{1\ thyroid} = 0.003$ Gy^{-1} and $\alpha_2 = 0.25$ Gy^{-2} were assumed, resulting in $\beta_{1\ breast}$, $\beta_{2\ breast}$, $\beta_{1\ thyroid}$ and $\beta_{2\ thyroid}$ values of 3.24x10^{-3}, 0.07, 1x10^{-3} and 0.08, respectively[74,76]. The tissue volumes are given (section 5.2.1).

Specific parameters are given in the BEIR VII Phase II report[75] for modelling female breast and thyroid cancer risks. For the given ERR parameters $\beta = 1.05$ (0.28, 3.9 95% CI), γ = -0.83 and $\eta = 0$, the thyroid cancer risk in females is given by:

$$ERR = D\ 1.05\ \exp[-0.083(e-30)]$$

The ERR model, with $\beta = 0.51$ (0.28, 0.83 95% CI), $\gamma = 0$ and η = -2.0, results in the risk of female breast cancer:

$$ERR = D\ 0.51\ (\alpha/60)^{-2}$$

For the given parameters $\beta = 9.4$ (6.7, 13.3 95% CI), γ = -0.51 and $\eta = 1.1$, the EAR for female breast cancer is given by:

$$EAR = D\ 9.4\ \exp[-0.05(e-30)](\alpha/60)^{1.1}$$

These models were evaluated for exposed ages, e = 40 and 50 years and attained ages 20 years later, α = 60 and 70 years.

The risk of radiation induced cancer due to CBCT was assessed for two common imaging schemes: daily (n=25) and imaging the first three days followed by weekly CBCT (n=7). The CT associated risk was calculated assuming only one CT was performed.

5.3 Results

5.3.1 CT & CBCT Imaging

The mean dose recorded (95% CI) from CBCT and CT acquisition is given in Table 5.2. The dose to the contralateral breast from CT imaging is approximately uniform across the volume. This is to be expected due to the helical nature of the image acquisition. Similar results were seen within the imaging field for 360° CBCT. Contralateral breast sub-volumes 3, 6 and 8 were outside of the imaging field for CBCT acquisition and this is reflected in the results. The MOSFET signal at CBCT is poor due to the low X-ray tube current and the attenuation of the epoxy bulb.

Table 5.2: Breast Imaging dose recorded from a single CBCT and CT scan.

Imaging Dose (cGy)				
	CBCT		CT	
Region	MOSFET	XR-QA2	MOSFET	XR-QA2
Thyroid	0.09 ± 0.18	0.34 ± 0.04	1.18 ± 0.13	1.94 ± 0.14
1	0.27 ± 0.33	1.18 ± 0.01	0.77 ± 0.34	1.74 ± 0.05
2	0.10 ± 0.11	1.15 ± 0.04	1.00 ± 0.38	1.95 ± 0.12
3	0.00 ± 0.00	0.34 ± 0.02	1.51 ± 0.67	2.50 ± 0.11
4	0.57 ± 0.29	1.08 ± 0.02	0.82 ± 0.26	1.45 ± 0.06
5	0.49 ± 0.21	1.00 ± 0.01	0.31 ± 0.20	1.90 ± 0.09
6	0.04 ± 0.08	0.24 ± 0.07	1.28 ± 0.81	2.14 ± 0.13
7	0.47 ± 0.15	0.94 ± 0.01	1.27 ± 0.52	1.61 ± 0.20
8	0.00 ± 0.00	0.31 ± 0.02	1.12 ± 0.28	2.01 ± 0.29

5.3.2 Treatment Delivery

The mean of the three single fraction deliveries and the associated uncertainty of the mean (95% CI) were calculated. The dose to the sub-volumes of the contralateral breast and thyroid from the five respective plans are tabulated for film (Table 5.3) and MOSFET dosimeters (Table 5.4) and represented graphically in Figure 5.5. The maximum dose measured is expressed as a percentage of the prescribed dose (Table 5.3 and 5.4 for film and MOSFETs, respectively). The highest dose was recorded at the three points closest to the treatment field for all treatment techniques, as expected. The physical wedge plan resulted in the largest dose to the contralateral breast and thyroid which is in agreement with reported studies. This is due to the increased scatter from the physical wedge.

Table 5.3: The total dose to the thyroid and contralateral breast as measured using EBT2 film. The total dose was calculated from the measured dose in a single fraction multiplied by the number of fractions ($n = 25$). The mean of three measurements (95% CI) is recorded and the maximum dose a sub-volume received is given (max dose). Regions 1-8 represent the contralateral breast sub-volumes.

Treatment Delivery Concomitant Dose (Gy) - film					
Region	SS 6MV	SS 10MV	EDW 6MV	EDW 10MV	PW
Thyroid	0.50 ± 0.21	0.68 ± 0.28	0.73 ± 0.14	0.47 ± 0.43	1.00 ± 0.16
1	4.47 ± 0.37	3.46 ± 0.11	4.29 ± 0.14	4.00 ± 0.08	4.56 ± 0.02
2	4.55 ± 0.32	3.51 ± 0.56	3.82 ± 0.27	4.44 ± 0.06	4.65 ± 0.17
3	3.38 ± 0.17	2.55 ± 0.11	2.06 ± 0.45	3.21 ± 0.39	3.63 ± 0.21
4	1.33 ± 0.23	1.01 ± 0.16	2.08 ± 0.30	2.01 ± 0.03	2.59 ± 0.22
5	1.47 ± 0.25	1.08 ± 0.35	1.83 ± 0.29	1.80 ± 0.37	2.67 ± 0.09
6	1.11 ± 0.12	0.88 ± 0.12	1.24 ± 0.09	1.35 ± 0.19	2.09 ± 0.09
7	0.34 ± 0.31	0.50 ± 0.16	0.78 ± 0.16	0.93 ± 0.33	0.94 ± 0.17
8	0.24 ± 0.18	0.28 ± 0.18	0.51 ± 0.31	0.54 ± 0.27	0.56 ± 0.17
Max dose	4.55 (10.1%)	3.51 (7.8%)	4.29 (9.5%)	4.44 (9.9%)	4.65 (10.3%)

Table 5.4: The total dose to the thyroid and contralateral breast as measured using MOSFET dosimeters. The total dose was calculated from the dose reading in a single fraction multiplied by the number of fractions (n = 25). The mean of three measurements (95% CI) is recorded and the maximum dose a sub-volume received is displayed (max dose). Regions 1-8 represent the contralateral breast sub-volumes.

Treatment Delivery Concomitant Dose (Gy) - MOSFET					
Section	SS 6MV	SS 10MV	EDW 6MV	EDW 10MV	PW
Thyroid	0.93 ± 0.32	1.42 ± 0.51	1.84 ± 0.16	1.09 ± 0.14	1.82 ± 0.18
1	2.64 ± 0.11	2.95 ± 0.40	0.74 ± 1.31	3.99 ± 0.33	4.96 ± 0.06
2	2.73 ± 0.08	2.93 ± 0.21	2.47 ± 0.17	3.78 ± 0.12	3.79 ± 0.19
3	2.00 ± 0.10	1.45 ± 0.12	1.09 ± 0.03	2.09 ± 0.58	3.12 ± 1.03
4	0.51 ± 0.36	0.49 ± 0.25	1.31 ± 0.19	1.40 ± 0.10	2.12 ± 0.15
5	0.73 ± 0.80	0.20 ± 0.36	0.97 ± 0.48	0.78 ± 0.30	1.63 ± 0.22
6	0.20 ± 0.12	0.40 ± 0.11	0.67 ± 0.05	0.24 ± 0.14	2.06 ± 0.34
7	0.17 ± 0.08	0.00 ± 0.00	0.15 ± 0.27	0.28 ± 0.26	0.39 ± 0.37
8	0.06 ± 0.11	0.14 ± 0.09	0.00 ± 0.00	0.00 ± 0.00	0.16 ± 0.12
Max dose	2.73 (6.1%)	2.95 (6.6%)	2.47 (5.4%)	3.99 (8.9%)	4.96 (11.0%)

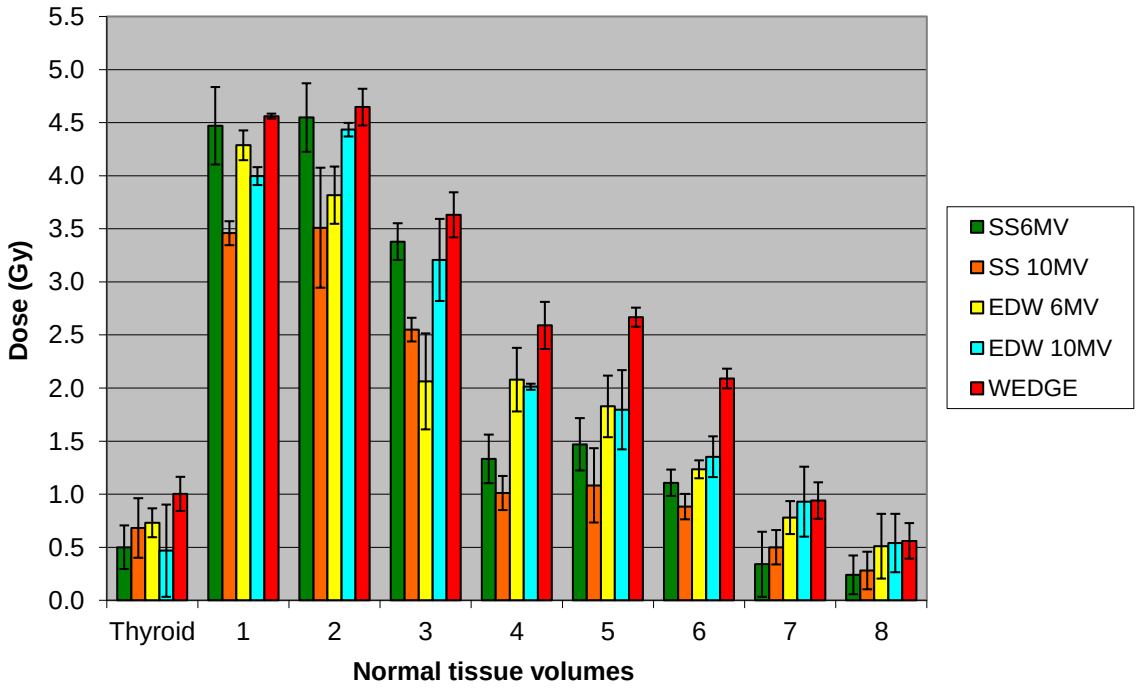

(a) EBT2 film measurements

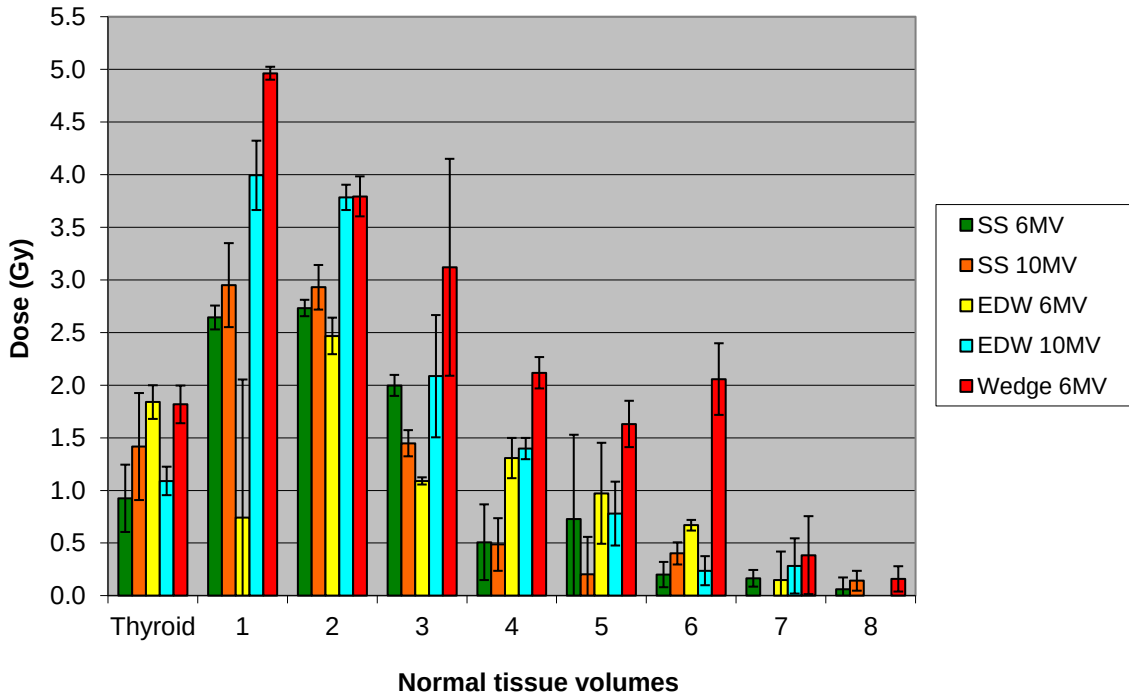

(b) MOSFET measurements

Figure 5.5: A comparison between the measured doses to the normal tissue volumes from the five treatment techniques: (a) EBT2 film and (b) MOSFETs. The recorded doses decrease with increasing distance from the treatment field. Normal tissue volumes 1-8 correspond to the contralateral breast sub-volumes.

The dose to the points of interest (95% CI) and the mean DVH thyroid dose extracted from Pinnacle^3 are given in Table 5.5. The TPS dose and the measured doses for each treatment technique are compared in Figure 5.6 and 5.7.

Table 5.5: The POI doses predicted in the TPS to the normal tissue volumes over the course of treatment. Dose to the surface of the phantom and at 1 mm depth are given. The DVH mean dose to the thyroid (DVH_{mean}) volume is given. Points 1-8 correspond to the contralateral breast sub-volumes with the same numbering.

Pinnacle^3 Dose (Gy)						
Region	Point Depth	SS 6MV	SS 10MV	EDW 6MV	EDW 10MV	PW
DVH_{mean}	-	0.34	0.21	0.31	0.20	0.53
Thyroid	surface	0.48 ± 0.06	0.30 ± 0.04	0.37 ± 0.07	0.36 ± 0.01	0.87 ± 0.03
	1 mm	0.51 ± 0.03	0.33 ± 0.02	0.43 ± 0.03	0.39 ± 0.01	0.93 ± 0.01
1	surface	1.22 ± 0.05	1.14 ± 0.05	1.77 ± 0.04	1.21 ± 0.26	1.46 ± 0.24
	1 mm	1.32 ± 0.03	1.02 ± 0.05	1.73 ± 0.03	1.46 ± 0.03	1.86 ± 0.03
2	surface	0.85 ± 0.28	0.78 ± 0.13	1.24 ± 0.24	1.33 ± 0.15	1.69 ± 0.24
	1 mm	1.17 ± 0.15	0.95 ± 0.06	1.67 ± 0.08	1.64 ± 0.03	2.06 ± 0.03
3	surface	0.97 ± 0.04	0.40 ± 0.12	1.05 ± 0.23	0.99 ± 0.10	1.21 ± 0.11
	1 mm	0.92 ± 0.02	0.57 ± 0.03	1.25 ± 0.05	1.21 ± 0.02	1.44 ± 0.01
4	surface	0.10 ± 0.02	0.08 ± 0.01	0.20 ± 0.01	0.09 ± 0.02	0.14 ± 0.03
	1 mm	0.11 ± 0.01	0.10 ± 0.01	0.22 ± 0.01	0.11 ± 0.02	0.16 ± 0.02
5	surface	0.14 ± 0.02	0.12 ± 0.01	0.25 ± 0.01	0.12 ± 0.03	0.23 ± 0.02
	1 mm	0.17 ± 0.00	0.14 ± 0.00	0.28 ± 0.00	0.16 ± 0.03	0.24 ± 0.01
6	surface	0.04 ± 0.01	0.04 ± 0.01	0.14 ± 0.02	0.13 ± 0.01	0.06 ± 0.02
	1 mm	0.06 ± 0.01	0.05 ± 0.01	0.14 ± 0.05	0.14 ± 0.01	0.08 ± 0.02
7	surface	0.09 ± 0.01	0.04 ± 0.01	0.08 ± 0.01	0.04 ± 0.01	0.08 ± 0.01
	1 mm	0.09 ± 0.01	0.05 ± 0.01	0.09 ± 0.01	0.03 ± 0.01	0.08 ± 0.01
8	surface	0.05 ± 0.02	0.04 ± 0.01	0.03 ± 0.01	0.04 ± 0.01	0.05 ± 0.02
	1 mm	0.06 ± 0.01	0.03 ± 0.01	0.03 ± 0.01	0.04 ± 0.01	0.04 ± 0.02

The film most often reads higher than the MOSFETs, with the variance increasing with increasing distance from the treatment field. Across the five plans, the average MOSFET dose was 71, 51 and 29% of the film dose for the medial, middle and lateral sub-volumes, respectively. The PW plan shows the best agreement between MOSFET and film measurements (76%), while 6MV EDW shows the worst at 42%. However, the disparity between MOSFET and film results was $\leq$ 4.5 cGy for the middle and lateral sub-volumes. For the thyroid, a direct comparison can not be made between MOSFET and film measurements as

the MOSFETs were placed on the phantom surface while the films were placed at depth and parallel to the incident beam. However, the results are in the same order of magnitude.

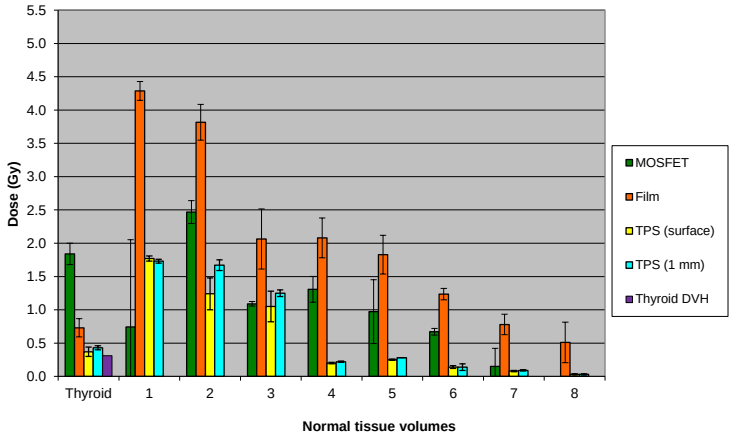

(a) Enhanced Dynamic Wedge 6MV

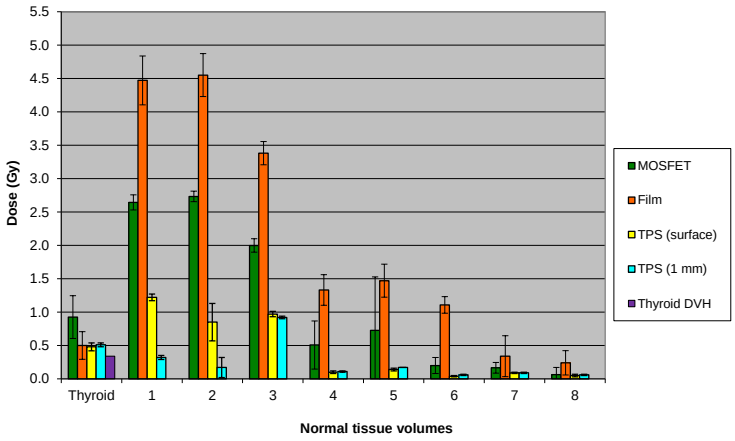

(b) Step and Shoot 6MV

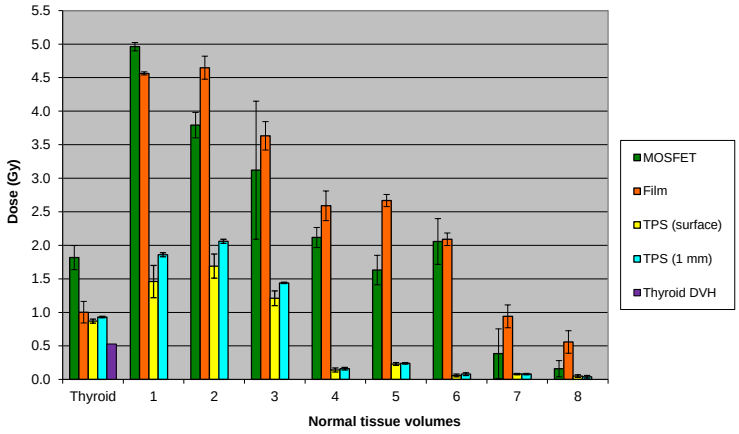

(c) Physical Wedge 6MV

Figure 5.6: A comparison between MOSFET, Gafchromic film and TPS dose to the normal tissue volumes from 6MV treatment techniques. Normal tissue volumes 1-8 correspond to the contralateral breast sub-volumes.

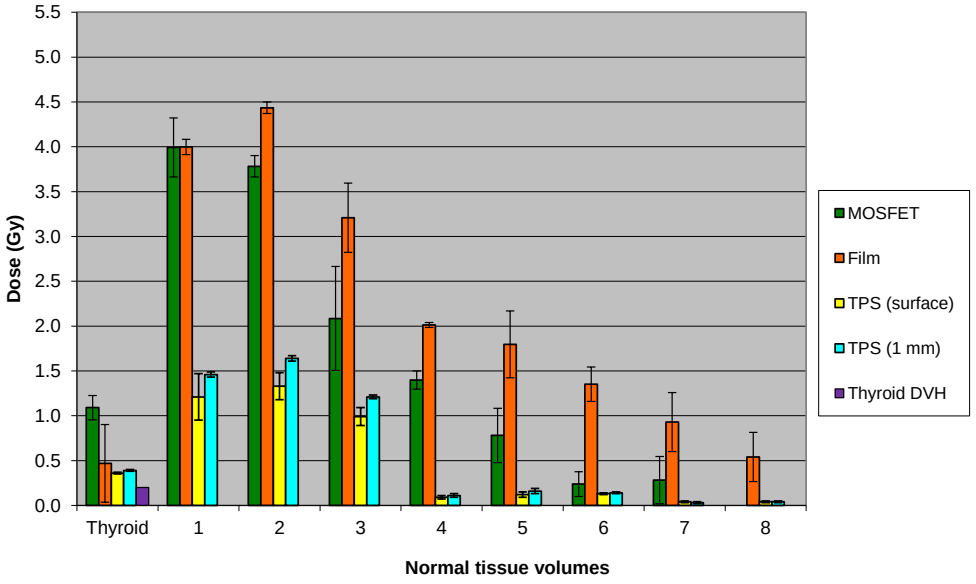

(a) Enhanced Dynamic Wedge 10MV

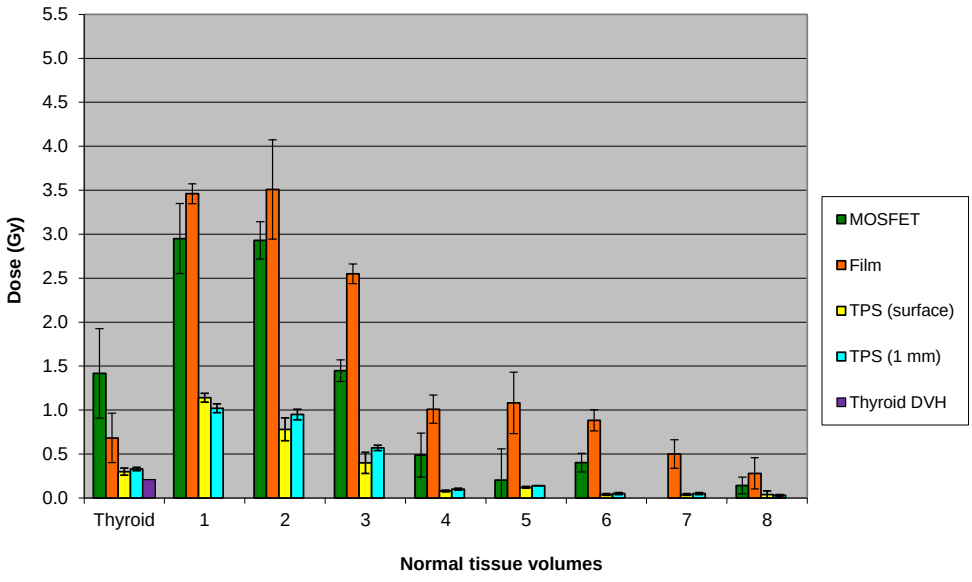

(b) Step and Shoot 10MV

Figure 5.7: A comparison between MOSFET, Gafchromic film and TPS dose to the normal tissue volumes from 10MV treatment techniques. Normal tissue volumes 1-8 correspond to the contralateral breast sub-volumes.

5.3.3 Risk Analysis

The risk of radiation induced cancer due to the accumulative dose to healthy tissue a patient receives while undergoing treatment was calculated based on a worst case scenario, i.e., the Gafchromic film measurements were used. The maximum dose received during CT and CBCT acquisition was assessed when using the ERR and EAR risk models and the risk was evaluated for 20 years post exposure and based on the assumption that the patient was treated at either 40 or 50 years of age (e = 40, 50y, attained age α = 60, 70y). The accumulative risk, with contributions from CT, CBCT and treatment, was determined based on the competition model risk estimates. The calculated risks are given in Table 5.6. In summary, the risk of radiotherapy to the breast causing cancer in the contralateral breast, as determined using the competition model, is approximately 1.2% averaged over all cases and 0.2% for inducing thyroid carcinoma.

Table 5.6: Radiation induced contralateral breast and thyroid cancer risk estimates using the competition, ERR and EAR risk models. EAR and ERR were calculated at 20 years post treatment for age at treatment of 40 or 50 years (e = 40, 50y and α = 60, 70y). The results are given as 40y / 50y. A worst case scenario was assumed by using the maximum doses delivered at CT and CBCT acquisition. The accumulative risk from CT, daily CBCT and treatment is considered.

Radiation Induced Cancer Risk Estimates				
Risk Model	Radiation Source		Cancer site	
			Contralateral Breast	Thyroid
Competition Model	Treatment	SS 6MV	1.04%	0.15%
		SS 10MV	0.98%	0.19%
		EDW 6MV	1.18%	0.20%
		EDW 10MV	1.23%	0.14%
		PW	1.34%	0.26%
	CBCT	*n = 7*	0.069%	0.008%
		n = 25	0.210%	0.028%
	CT		0.021%	0.006%
ERR (40y / 50y)	CBCT	*n = 7*	0.048% / 0.035%	0.011% / 0.005%
		n = 25	0.171% / 0.124%	0.039% / 0.017%
	CT		0.013% / 0.009%	0.009% / 0.004%
EAR (40y / 50y)[1]	CBCT	*n = 7*	0.53 / 1.37	-
		n = 25	1.91 / 0.38	-
	CT		0.14 / 0.10	-
Accumulative Risk		SS 6MV	1.07%	0.15%
		SS 10MV	1.01%	0.19%
		EDW 6MV	1.20%	0.20%
		EDW 10MV	1.25%	0.14%
		PW	1.36%	0.26%

[1] EAR expressed in cases per 10,000 people per year.

5.4 Discussion

The calculated accumulative risk of radiation induced cancer to the contralateral breast when treating early stage breast carcinoma was found to be 1.2% (range 1.1 - 1.4%). This risk estimate takes into consideration the dose from treatment, imaging for planning and pretreatment imaging. Treatment delivery using physical wedges resulted in the nominally greatest risk, 1.4%. For a prescribed dose of 45 Gy in 25 fractions, the higher doses were measured at the points closest to the treatment field, with the maximum dose to the contralateral breast of 4.55 ± 0.32, 3.51 ± 0.56, 4.29 ± 0.14, 4.44 ± 0.06 and 4.96 ± 0.06 Gy for SS 6MV, SS 10MV, EDW 6MV, EDW 10MV and PW treatment delivery, respectively. These doses correspond to 10.1%, 7.8%, 9.5%, 9.9% and 11.0% of the prescribed treatment dose and are in agreement with doses previously reported. Prabhakar *et al.*[4] investigated the contralateral breast surface dose due to wedged (physical and dynamic) and unwedged 6MV tangential fields using MOSFET detectors and reported doses of up to 15.3% with 60° physical wedges fitted. Dose conformity using 15° physical and enhanced dynamic wedges resulted in maximum surface doses of 10.5% and 9.8%, respectively. Johansen *et al.*[23] employed DVH analysis to assess the dose to the contralateral breast for 16 patients treated with 50 Gy in 2 Gy fractions using tangential fields. The mean of the maximum contralateral breast doses for the 16 patients was 5.4 Gy (10.8%). Bhatnagar *et al.*[5] reported surfaces doses of 7.7% of the prescribed dose using thermoluminescent dosimeters positioned on the patient's contralateral breast, 4 cm from the centre of the medial border of the tangent field. Mean doses to the contralateral volume of 0.3 - 3.0 Gy have been reported[23–25].

Several studies have assessed the role of radiation treatment in the development of contralateral breast cancer. A cohort study evaluating 529 contralateral breast cancers which developed at least 8 years after initial breast cancer diagnosis, with an average patient exposure age of 51 years and an estimated mean contralateral breast dose of 2.51 Gy, found little risk of radiation induced breast cancer for an age of first treatment 50+ years[107]. Another study evaluated 655 cases of second breast cancer with an estimated mean dose to the contralateral breast of 3.02 Gy. The association between contralateral breast cancer and radiotherapy was minimal, however, for patients less than 44 years of age at initial diagnosis,

a stronger correlation was observed. The incidence of second cancers was not linked to radiotherapy for treatment age 45+ years. Boice *et al.*[24] concluded that the risk of secondary breast cancer due to radiotherapy is largely dependent on age at treatment.

The contralateral breast cancer risk associated with daily CBCT was 0.2%, which was reduced by approximately 1/3 when the alternative pretreatment imaging protocol was assumed (image the first three days and then weekly). For the Low Dose Thorax standard imaging protocol, surface dose measurements using XR-QA2 film, made within the imaging field, ranged 0.94 - 1.18 cGy. This is comparable to the dose, ranging 0.65 - 0.95 cGy, measured by Ueltzhöffer *et al.*[25] using an ionisation chamber. Despite the low risk, imaging parameters, such as gantry start and stop angle, mA and kVp, can be optimised to further reduce the dose to the healthy tissue while maintaining adequate image quality[25]. An annual increase of 1.9 breast cancers per 10,000 people receiving daily CBCT ($n = 25$) and 0.1 breast cancers per 10,000 breast CT scans was estimated. This equates to an annual increase of 1 breast cancer per 70,000 breast CT scans.

Concomitant dose of up to 1.0 Gy was measured at the thyroid from treatment delivery. Thyroid doses of 0.3 and 1.9 cGy per scan were recorded for CBCT and CT, respectively. However, the risk of thyroid cancer as a result of radiotherapy and the associated imaging for breast carcinoma was found to be negligible, 0.2% (range 0.1 - 0.3%). Huang *et al.*[101], in a retrospective population based study, identified 194,798 women diagnosed with breast cancer, of which 48,495 were treated with radiotherapy. 140 subsequent thyroid cancers developed (28 in the group treated with radiotherapy) with a follow up of at least 10 years. Nevertheless, no significant increase in the risk of thyroid cancer was observed for patients treated with radiation therapy compared to those not having received radiotherapy and the general population. Similarly, no increased incidence of radiation related secondary thyroid cancer was observed in a cohort study involving 64,782 women who underwent surgery for breast carcinoma, of which 33,763 received adjuvant radiotherapy[108]. Although radiotherapy for breast cancer is not associated with the risk of thyroid cancer, an increased prevalence of thyroid disease, such as nontoxic goiter and Hashimoto's thyroiditis, has been observed[100,109]. The risk of thyroid dysfunction following radiotherapy is related to the volume of the thyroid

irradiated[99].

There are several limitations in the approach used to estimate the risk of second malignancies. One limitation is the availability of the coefficients required for the competition model[74]. α/β ratios are based on clinical studies and vary depending on treatment dose, treatment fractionation regime and stipulated end points. However, more significantly, the model requires α_1 values which are difficult to come by. In this study, ICRP nominal risk coefficients were used as a best estimate. Additionally, the competition model is intended to be used with dose volume histogram data to sum the effects in each dose interval across the volume of concern. A slightly different methodology was used in this work; the sum of the effect in each delineated sub-volume was calculated. Furthermore, EAR and ERR model parameters are largely based on pooled analysis population studies of atomic bomb survivors and as such, the beneficial effects of fractionation are not accounted for.

In summary, the risk of radiation induced contralateral breast and thyroid cancer, following doses received while undergoing radiotherapy for breast carcinoma, was found to be minimal. Treatment delivery using physical wedges for dose conformity resulted in the highest second cancer risk.

5.5 Conclusion

Maximum contralateral breast doses of 4.55 ± 0.32, 3.51 ± 0.56, 4.29 ± 0.14, 4.44 ± 0.06 and 4.96 ± 0.06 Gy were measured for SS 6MV, SS 10MV, EDW 6MV, EDW 10MV and PW treatment delivery, respectively. These doses correspond to 10.1%, 7.8%, 9.5%, 9.9% and 11.0% of the prescribed treatment dose. The risk of contralateral breast malignancies following radiation exposure due to breast imaging and treatment, was found to be 1.1 - 1.4%, with treatment delivery using physical wedges resulting in the greatest risk. The associated risk of thyroid carcinoma was trivial (0.1 - 0.3%).

Nevertheless, the ALARA[76] principle should be adopted when implementing pretreatment imaging protocols and when considering alternative treatment techniques for dose conformity, thereby reducing the dose to healthy tissue surrounding the target volume and consequently, unnecessary side effects.

Chapter 6

Discussion and Conclusions

6.1 Discussion

The aim of this work was to assess the risk of radiation induced secondary malignancies to normal tissue lying out of the treatment field for patients who are treated at a relatively young age and whose primary cancer treatment has a good prognosis, thus accounting for the time delay for radiation induced cancers to occur. The risk of thyroid and contralateral breast carcinoma from early stage breast radiotherapy and the risk of contralateral testicular carcinoma from seminoma radiotherapy were investigated. The dose to healthy tissue from imaging for planning, pretreatment imaging and treatment related scatter was measured using MOSFET detectors and Gafchromic film. To the author's knowledge this is the first work to compare Gafchromic film and MOSFET dosimeters for investigating the total concomitant treatment related dose and associated risk.

For seminoma cancer radiotherapy, dose to the contralateral testis was measured resulting from a prescribed dose to the paraaortic region including the ipsilateral and common iliac lymph nodes and that to the paraaortic region only. Additionally, dose with and without gonadal shielding was assessed. The mean dose to the contralateral testis for a total prescription of 20.0 Gy to the paraaortic region was 0.30 $\pm$ 0.08 Gy and 0.31 $\pm$ 0.04 Gy with and without lead shielding, respectively. For a prescribed dose of 30.0 Gy to the extended PA region, the mean testicular dose was 0.61 $\pm$ 0.11 Gy and 0.68 $\pm$ 0.39 Gy with and without

shielding, respectively. These doses are slightly higher than those previously reported[19,83], nevertheless, the accumulative risk of radiation induced cancer, taking into consideration all imaging and treatment related dose and the use of gonadal shielding, was found to be 0.4% and 0.2% for dogleg and paraaortic treatment fields. These risks are approximately 4 - 13 times less than the secondary testicular cancer incidence reported in the literature[16,17,84,85].

The dose to the contralateral breast was measured for five different treatment techniques, with a maximum measured dose of 4.55 ± 0.32, 3.51 ± 0.56, 4.29 ± 0.14, 4.44 ± 0.06 and 4.96 ± 0.06 Gy for SS 6MV, SS 10MV, EDW 6MV, EDW 10MV and PW treatment delivery, respectively. Doses of up to 11% of the prescribed treatment were measured near the edge of the treatment field, which is in agreement with previously reported measurements[4,5,23]. The calculated approximate accumulative risk of radiation induced cancer to the CB when treating early stage breast carcinoma was found to be 1.1 - 1.4%, depending on the treatment technique used.

Concomitant dose of up to 1.0 Gy was measured at the thyroid from radiotherapy treatment for early stage breast carcinoma. Thyroid doses of 0.3 and 1.9 cGy per scan were recorded for CBCT and CT, respectively. Nevertheless, the resulting accumulative risk of thyroid cancer was found to be negligible, 0.2%.

6.2 Limitations of the Approach

There are several limitations in the methodology used in this work including, but not limited to, the availability of risk model parameters and the uncertainty of the energy spectrum in the periphery of the treatment fields.

The competition risk model requires model parameter α_1 which is not easily obtainable in the literature. Consequently, ICRP nominal risk coefficients were used as a suitable alternative. Additionally, the competition model is designed to be used with dose volume histogram data from the treatment planning system to sum the effects of the dose per volume across the organ at risk, whereas, in this work, measured organ at risk doses to specified volumes were used. The excess relative risk and excess absolute risk model parameters

were not available for testicular cancer risk assessment and as such model parameters for all solid cancers were used as a best estimate. Furthermore, the EAR and ERR models do not account for fractionation in treatment regimes.

The energy spectrum of peripheral dose has been investigated by several authors[62,110–112] and is dependent on beam energy, field size, distance from the field edge and linear accelerator model. Although EBT2 Gafchromic film and MOSFET detectors demonstrate little energy dependence in the MV energy range[47,56], internal scatter, which is a major contributor to the dose in the near periphery of treatment fields, has energy spectral peaks near 500 keV for 6 and 15 MV beams[62]. EBT2 film is designed for use in beams of energy down to 50 keV, however, small variations in the chemical composition of the film which occur over time can result in large over- or under responding of the film[113]. Future work would include determining the energy spectrum of the scatter at the radiosensitive organs lying out of the treatment field in order to accurately calibrate the dosimeters intended to measure the scatter dose.

TN-1002RD MOSFETs and Gafchromic film were found to be suitable dosimeters for measuring dose in the kV and MV range. The accuracy of MOSFET measurements decrease at distances > 5 cm from the treatment field, i.e. regions of low dose. The reproducibility of MOSFETs for low dose deliveries was 26.6, 50.4 and 18.1% in 150 kVp, 180 kVp and 6 MV beams, respectively. Gafchromic film has good precision at low doses. The reproducibility of EBT2 was 1.0% for beam energy 6 MV. For 150 and 180 kVp, the uncertainty of XR-QA2 film was 3.1 and 3.0%, respectively. For exposures above 3 cGy, the accuracy of XR-QA2 is within 5% for measurements made within 150 and 180 kVp beams. EBT2 Gafchromic film overestimates the dose by approximately 20% in the peripheral regions of MV beams.

Despite the relatively large uncertainties for some dose measurements, the overall secondary cancer risk remains low.

6.3 Conclusion

The risk of radiation induced second malignancies was assessed for healthy tissue lying near the treatment field, taking into consideration radiation dose associated with planning imaging (CT), pretreatment imaging (CBCT) and treatment. The risk of thyroid and contralateral breast carcinoma from early stage breast radiotherapy and the risk of contralateral testicular carcinoma from seminoma radiotherapy were investigated. The maximum surface dose to the remaining testis, contralateral breast and thyroid was 0.68, 4.96 and 1.0 Gy, respectively. With gonadal shielding fitted to reduce the testicular dose, the accumulative risk of radiation induced testicular cancer was found to be 0.4% and 0.2% for dogleg and paraaortic treatment fields, respectively. The accumulative risk of radiation induced second malignancies to the CB was found to be 1.1 - 1.4%, depending on the treatment technique used. Dose conformity using physical wedges resulted in the highest CB dose and therefore the highest risk. The resulting accumulative risk of thyroid cancer from radiotherapy treatment for early stage breast carcinoma was found to be minimal, 0.2%. Despite the minor risk of radiation induced carcinoma to the assessed radiosensitive tissues, when considering possible treatment techniques and/or introducing pretreatment imaging protocols, the dose to the normal tissue should be kept as low as reasonably achievable.

Acknowledgements

This work would not have been possible without the guidance and assistance of several individuals who in one way or another contributed to the completion of this study.

First and foremost, I am grateful to my supervisor at the University of Canterbury, Dr. Juergen Meyer, whose thoughtful guidance kept me on track.

I owe my deepest gratitude to Christine Thompson, my thesis supervisor within the Auckland City Hospital, for her never ending source of support and encouragement.

I am indebted to my many colleagues who supported me and made time to answer my endless questions; Allan Stewart, Deirdre Hutton, Gerard Bengua and Rick Sims, to name a few. Additionally, I would like to thank Rick and Deirdre for reading first drafts and providing helpful feedback.

Many radiation therapists offered clinical advice and assisted me in carrying out specific tasks for which I am truly grateful. There are too many to mention them all by name, although I would like to make special mention of Tania Ferguson, Paula Tallon, Sarah Woodroofe and Tereza Austin. Also to Kim Robinson and Geoff Logan, whose knowledge in the Mould Room provided invaluable support.

Lastly, to my wonderful friends who still invite me out despite having numerous invites declined because I needed to work on my thesis. I am grateful you are still around.

Bibliography

[1] International Speciality Products Gafchromic® EBT2. Self-developing film for radiotherapy dosimetry, Wayne, NJ, USA. 2009.

[2] M Kan, L Leung, W Wong, and N Lam. Radiation dose from cone beam computed tomography for image-guided radiation therapy. *International Journal of Radiation Oncology,Biology,Physics*, 70(1):272–279, 2008.

[3] JR Mayo, J Aldrich, and NL Müller. Radiation exposure at chest CT: A statement of the Fleischner Society. *Radiology*, 228(1):15–21, 2003.

[4] R Prabhakar, K Haresh, P Julka, T Ganesh, et al. A study on contralateral breast surface dose for various tangential field techniques and the impact of set-up error on this dose. *Australasian Physical & Engineering Science in Medicine*, 30:42–45, 2007.

[5] AK Bhatnagar, E Brandner, D Sonnik, A Wu, et al. Intensity-modulated radiation therapy (IMRT) reduces the dose to the contralateral breast when compared to conventional tangential fields for primary breast irradiation: initial report. *Breast Cancer Research and Treatment*, 10(1):41–46, 2006.

[6] DL Preston, E Ron, S Tokuoka, S Funamoto, et al. Solid cancer incidence in atomic bomb survivors: 19581998. *Radiation Research*, 168(1):1–64, 2007.

[7] DL Preston, A Mattsson, E Holmberg, R Shore, et al. Radiation effects on breast cancer risk: A pooled analysis of eight cohorts. *Radiation Research*, 158(2):220–235, 2002.

[8] L Krestinina, F Davis, EV Ostroumova, SB Epifanova, et al. Solid cancer incidence and low-dose-rate radiation exposures in the Techa River cohort: 1956-2002. *International Journal of Epidemiology*, 36(5):1038–1046, 2007.

[9] E Ron. Cancer risks from medical radiation. *Health Physics*, 85(1):47–59, 2003.

[10] LB Travis, RE Curtis, and BF Hankey. Second malignancies after testicular cancer. *Journal of Clinical Oncology*, 13(2):533–534, 1995.

[11] AI Neugut, T Murray, J Santos, H Amols, et al. Increased risk of lung cancer after breast cancer radiation therapy in cigarette smokers. *Cancer*, 73(6):1615–1620, 1994.

[12] SL Hancock, MA Tucker, and RT Hoppe. Breast cancer after treatment of Hodgkin's Disease. *Journal of the National Cancer Institute*, 85(1):25–31, 1993.

[13] AJ Swerdlow, JA Barber, GV Hudson, D Cunningham, et al. Risk of second malignancy after Hodgkin's Disease in a collaborative British cohort: The relation to age at treatment. *Journal of Clinical Oncology*, 18(3):498, 2000.

[14] DJ Brenner and EJ Hall. Computed tomography: An increasing source of radiation exposure. *New England Journal of Medicine*, 357(22):2277–2284, 2007.

[15] A Berrington de González, M Mahesh, K Kim, M Bhargavan, et al. Projected cancer risks from computed tomographic scans performed in the United States in 2007. *Archives of Internal Medicine*, 169(22):2071–2077, 2009.

[16] U Rüther, KP Dieckmann, R Bussar-Maatz, and F Eisenberger. Second malignancies following pure seminoma. *Oncology*, 58, 2000.

[17] A Hellbardt, RO Mirimanoff, M Obradovic, B Mermillod, and JP Paunier. The risk of second cancer (SC) in patients treated for testicular seminoma. *International Journal of Radiation Oncology,Biology,Physics*, 18(6):1327–1331, 1990.

[18] E Huyghe, T Matsuda, M Daudin, C Chevreau, et al. Fertility after testicular cancer treatments. *Cancer*, 100(4):732–737, 2004.

[19] S Bieri, M Rouzaud, and R Miralbell. Seminoma of the testis: Is scrotal shielding necessary when radiotherapy is limited to the para-aortic nodes? *Radiotherapy and Oncology*, 50(3):349–353, 1999.

[20] M Serge, A Costa, and JL Lagrange. Protection of testes during radiation treatment by irregular and focused fields of 25 MV X-rays: In vivo evaluation of the absorbed dose. *Medical Dosimetry*, 20(4):269–273, 1995.

[21] M Stovall, SA Smith, BM Langholz, JD Boice, et al. Dose to the contralateral breast from radiotherapy and risk of second primary breast cancer in the WECARE study. *International Journal of Radiation Oncology, Biology, Physics*, 72(5):1021–1030, 2008.

[22] TM Williams, JM Moran, SH Hsu, R Marsh, et al. Contralateral breast dose after whole-breast irradiation: An analysis by treatment technique. *International Journal of Radiation Oncology, Biology, Physics*, 82(5):2079–2085, 2012.

[23] S Johansen, J Vikström, MHB Hjelstuen, I Mjaaland, et al. Dose evaluation and risk estimation for secondary cancer in contralateral breast and a study of correlation between thorax shape and dose to organs at risk following tangentially breast irradiation during deep inspiration breath-hold and free breathing. *Acta Oncologica*, 50(4):563–568, 2011.

[24] JD Boice, EB Harvey, M Blettner, M Stovall, and JT Flannery. Cancer in the contralateral breast after radiotherapy for breast cancer. *New England Journal of Medicine*, 326(12):781–785, 1992.

[25] S Ueltzhoffer, P Zygmanski, J Hesser, W Hogele, et al. Clinical application of Varian OBI CBCT system and dose reduction techniques in breast cancer patients setup. *Medical Physics*, 37(6):2985–2998, 2010.

[26] M Mazonakis, H Varveris, J Damilakis, N Theoharopoulos, and N Gourtsoyiannis. Radiation dose to conceptus resulting from tangential breast irradiation. *International Journal of Radiation Oncology,Biology,Physics*, 55(2):386–391, 2003.

[27] PH Van der Giessen. Measurement of the peripheral dose for the tangential breast treatment technique with Co-60 gamma radiation and high energy X-rays. *Radiotherapy and Oncology*, 42(3):257–264, 1997.

[28] A Alzoubi, S Kandaiya, A Shukri, and E Elsherbieny. Contralateral breast dose from chest wall and breast irradiation: local experience. *Australasian Physical & Engineering Science in Medicine*, 33:137–144, 2010.

[29] KY Quach, J Morales, MJ Butson, AB Rosenfeld, and PE Metcalfe. Measurement of radiotherapy X-ray skin dose on a chest wall phantom. *Medical Physics*, 27(7):1676–1680, 2000.

[30] CF Chuang, LJ Verhey, and P Xia. Investigation of the use of MOSFET for clinical IMRT dosimetric verification. *Medical Physics*, 29(6):1109–1115, 2002.

[31] L Paelinck, N Reynaert, H Thierens, W De Neve, and C De Wagter. Experimental verification of lung dose with radiochromic film: comparison with Monte Carlo simulations and commercially available treatment planning systems. *Physics in Medicine and Biology*, 50(9):2055, 2005.

[32] N Tomic, S Devic, F DeBlois, and J Seuntjens. Reference radiochromic film dosimetry in kilovoltage photon beams during CBCT image acquisition. *Medical Physics*, 37(3):1083–1092, 2010.

[33] J Boivin, N Tomic, B Fadlallah, F DeBlois, and S Devic. Reference dosimetry during diagnostic CT examination using XR-QA radiochromic film model. *Medical Physics*, 38(9):5119–5129, 2011.

[34] O Rampado, E Garelli, and R Ropolo. Computed tomography dose measurements with radiochromic films and a flatbed scanner. *Medical Physics*, 37(1):189–196, 2010.

[35] T Kairn, N Hardcastle, J Kenny, R Meldrum, et al. EBT2 radiochromic film for quality assurance of complex IMRT treatments of the prostate: Micro-collimated IMRT, RapidArc, and TomoTherapy. *Australasian Physical & Engineering Science in Medicine*, 34:333–343, 2011.

[36] C He, M Geso, T Ackerly, and C Wong. Stereotactic dose perturbation from an aneurysm clip measured by Gafchromic® EBT film. *Australasian Physical & Engineering Science in Medicine*, 31:18–23, 2008.

[37] R Gotanda, T Katsuda, T Gotanda, A Tabuchi, H Yatake, and Y Takeda. Dose distribution in pediatric CT head examination using a new phantom with radiochromic film. *Australasian Physical & Engineering Science in Medicine*, 31:339–344, 2008.

[38] S Aldelaijan, S Devic, H Mohammed, N Tomic, et al. Evaluation of EBT-2 model GAFCHROMIC® film performance in water. *Medical Physics*, 37(7):3687–3693, 2010.

[39] C Andres, A del Castillo, R Tortosa, D Alonso, and R Barquero. A comprehensive study of the Gafchromic EBT2 radiochromic film. a comparison with EBT. *Medical Physics*, 37(12):6271–6278, 2010.

[40] M Butson, P Yu, T Cheung, and H Alnawaf. Energy response of the new EBT2 radiochromic film to X-ray radiation. *Radiation Measurements*, 45(7):836–839, 2010.

[41] T Aland, T Kairn, and J Kenny. Evaluation of a Gafchromic EBT2 film dosimetry system for radiotherapy quality assurance. *Australasian Physical & Engineering Science in Medicine*, 34:251–260, 2011.

[42] L Richley, AC John, H Coomber, and S Fletcher. Evaluation and optimization of the new EBT2 radiochromic film dosimetry system for patient dose verification in radiotherapy. *Physics in Medicine and Biology*, 55(9):2601, 2010.

[43] BD Lynch, J Kozelka, MK Ranade, JG Li, et al. Important considerations for radiochromic film dosimetry with flatbed CCD scanners and EBT GAFCHROMIC® film. *Medical Physics*, 33(12):4551–4556, 2006.

[44] M Martišíková, B Ackermann, and O Jäkel. Analysis of uncertainties in Gafchromic® EBT film dosimetry of photon beams. *Physics in Medicine and Biology*, 53(24):7013, 2008.

[45] S Devic, S Aldelaijan, H Mohammed, N Tomic, et al. Absorption spectra time evolution of EBT-2 model GAFCHROMIC™ film. *Medical Physics*, 37(5):2207–2214, 2010.

[46] O Rampado, E Garelli, S Deagostini, and R Ropolo. Dose and energy dependence of response of Gafchromic® XR-QA film for kilovoltage X-ray beams. *Physics in Medicine and Biology*, 51(11):2871, 2006.

[47] B Arjomandy, R Tailor, A Anand, N Sahoo, et al. Energy dependence and dose response of Gafchromic EBT2 film over a wide range of photon, electron, and proton beam energies. *Medical Physics*, 37(5):1942–1947, 2010.

[48] S Devic, J Seuntjens, E Sham, EB Podgorsak, et al. Precise radiochromic film dosimetry using a flat-bed document scanner. *Medical Physics*, 32(7):2245–2253, 2005.

[49] L Paelinck, W De Neve, and C De Wagter. Precautions and strategies in using a commercial flatbed scanner for radiochromic film dosimetry. *Physics in Medicine and Biology*, 52(1):231242, 2007.

[50] International Specialty Products (ISP). Correction protocol for Gafchromic EBT2 dosimetry film. 2009.

[51] SA Graham, DJ Moseley, JH Siewerdsen, and DA Jaffray. Compensators for dose and scatter management in cone-beam computed tomography. *Medical Physics*, 34(7):2691–2703, 2007.

[52] P Roxby, T Kron, F Foroudi, A Haworth, et al. Simple methods to reduce patient dose in a varian cone beam ct system for delivery verification in pelvic radiotherapy. *British Journal of Radiology*, 82(982):855–859, 2009.

[53] International Atomic Energy Agency. *Absorbed dose determination in photon and electron beams. An international code of practice.* Number No. 277 in Technical Reports Series. 1987.

[54] DJ Peet and MD Pryor. Evaluation of a MOSFET radiation sensor for the measurement of entrance surface dose in diagnostic radiology. *British Journal of Radiology*, 72(858):562–568, 1999.

[55] P Scalchi and P Francescon. Calibration of a MOSFET detection system for 6-MV in vivo dosimetry. *International Journal of Radiation Oncology,Biology,Physics*, 40(4):987–993, 1998.

[56] A Gopiraj, RS Billimagga, and V Ramasubramanian. Performance characteristics and commissioning of MOSFET as an in-vivo dosimeter for high energy photon external beam radiation therapy. *Reports of Practical Oncology and Radiotherapy*, 13(3):114–125, 2008.

[57] I Thomson, RE Thomas, and LP Berndt. Radiation dosimetry with MOS sensors. *Radiation Protection Dosimetry*, 6(1-4):121–124, 1983.

[58] M Soubra, J Cygler, and G Mackay. Evaluation of a dual bias dual metal oxide-silicon semiconductor field effect transistor detector as radiation dosimeter. *Medical Physics*, 21(4):567–572, 1994.

[59] C Ehringfeld, S Schmid, K Poljanc, C Kirisits, et al. Application of commercial mosfet detectors for in vivo dosimetry in the therapeutic X-ray range from 80 kV to 250 kV. *Phys Med Biol*, 50(2):289–303, 2005.

[60] K Bulinski and P Kukolowicz. Characteristics of metal oxide seimiconductor field effect transistors for application in radiotherapy. *Polish Journal of Medical Physics and Engineering*, 10(1):13–24, 2004.

[61] T Cheung, M Butson, and P Yu. MOSFET dosimetry in-vivo at superficial and orthovoltage X-ray energies. *Australasian Physical & Engineering Science in Medicine*, 26:81–83, 2003.

[62] N Chofor, D Harder, KC Willborn, and B Poppe. Internal scatter, the unavoidable major component of the peripheral dose in photon-beam radiotherapy. *Physics in Medicine and Biology*, 57(6):1733, 2012.

[63] ML Taylor, T Kron, and RD Franich. Assessment of out-of-field doses in radiotherapy of brain lesions in children. *International Journal of Radiation Oncology,Biology,Physics*, 79(3):927–933, 2011.

[64] M Taylor and T Kron. Consideration of the radiation dose delivered away from the treatment field to patients in radiotherapy. *Journal of Medical Physics*, 36(2):59–71, 2011.

[65] S Kry, M Salehpour, DS Followill, M Stovall, et al. Out-of-field photon and neutron dose equivalents from step-and-shoot intensity-modulated radiation therapy. *International Journal of Radiation Oncology,Biology,Physics*, 62(4):1204–1216, 2005.

[66] MC Lavallee, L Gingras, and L Beaulieu. Energy and integrated dose dependence of MOSFET dosimeter sensitivity for irradiation energies between 30 kV and ^{60}Co. *Medical Physics*, 33(10):3683–3689, 2006.

[67] SL Dong, TC Chu, GY Lan, TH Wu, et al. Characterization of high-sensitivity metal oxide semiconductor field effect transistor dosimeters system and LiF:Mg,Cu,P thermoluminescence dosimeters for use in diagnostic radiology. *Applied Radiation and Isotopes*, 57(6):883–891, 2002.

[68] T Giaddui, Y Cui, J Galvin, W Chen, et al. Characteristics of Gafchromic XRQA2 films for kV image dose measurement. *Medical Physics*, 39(2):842–850, 2012.

[69] RB Den, A Doemer, G Kubicek, G Bednarz, et al. Daily image guidance with cone-beam computed tomography forhead-and-neck cancer intensity-modulated radiotherapy: Aprospective study. *International Journal of Radiation Oncology,Biology,Physics*, 76(5):1353–1359, 2010.

[70] J Boda-Heggemann, F Lohr, F Wenz, M Flentje, and M Guckenberger. kV cone-beam CT-based IGRT. *Strahlentherapie und Onkologie*, 187:284–291, 2011.

[71] JP Bissonnette, TG Purdie, JA Higgins, W Li, and A Bezjak. Cone-beam computed tomographic image guidance for lung cancer radiation therapy. *International Journal of Radiation Oncology,Biology,Physics*, 73(3):927–934, 2009.

[72] M Josipovic, GF Persson, A Logadottir, B Smulders, et al. Translational and rotational intra- and inter-fractional errors in patient and target position during a short course of frameless stereotactic body radiotherapy. *Acta Oncologica*, 51(5):610–617, 2012.

[73] RB Case, JJ Sonke, DJ Moseley, J Kim, et al. Inter- and intrafraction variability in liver position in non-breath-hold stereotactic body radiotherapy. *International Journal of Radiation Oncology,Biology,Physics*, 75(1):302–308, 2009.

[74] A Daşu, I Toma-Daşu, J Olofsson, and M Karlsson. The use of risk estimation models for the induction of secondary cancers following radiotherapy. *Acta Oncologica*, 44(4):339–347, 2005.

[75] National Research Council Committee to Assess Health Risks from Exposure to Low Levels of Ionizing Radiation. *Health Risks from Exposure to Low Levels of Ionizing Radiation: BEIR VII Phase 2*. The National Academies Press, 2006.

[76] ICRP. The 2007 recommendations of the International Commission on Radiological Protection. *ICRP Publication 103, Ann. ICRP*, 37(2-4), 2007.

[77] J Ferlay, HR Shin, F Bray, D Forman, et al. GLOBOCAN 2008 v 1.2, cancer incidence and mortality worldwide: IARC CancerBase No.10, 2010.

[78] JE Livsey, B Taylor, N Mobarek, RA Cooper, et al. Patterns of relapse following radiotherapy for stage I seminoma of the testis: Implications for follow-up. *Clinical Oncology*, 13(4):296–300, 2001.

[79] P Warde, MK Gospodarowicz, T Panzarella, CN Catton, et al. Stage I testicular seminoma: Results of adjuvant irradiation and surveillance. *Journal of Clinical Oncology*, 13(9):2255–2262, 1995.

[80] N Boujelbene, A Cosinschi, N Boujelbene, K Khanfir, et al. Pure seminoma: A review and update. *Radiation Oncology*, 6(1):90, 2011.

[81] JF Fowler. The linear-quadratic formula and progress in fractionated radiotherapy. *British Journal of Radiology*, 62(740):679–694, 1989.

[82] A van der Kogel and M Joiner. *Basic Clinical Radiobiology*. A Hodder Arnold Publication. Hodder Arnold, 2009.

[83] KD Jacobsen, DR Olsen, K Fosså, and SD Fosså. External beam abdominal radiotherapy in patients with seminoma stage I: Field type, testicular dose, and spermatogenesis. *International Journal of Radiation Oncology,Biology,Physics*, 38(1):95–102, 1997.

[84] C Chao, PP Lai, JM Michalski, and CA Perez. Secondary malignancy among seminoma patients treated with adjuvant radiation therapy. *International Journal of Radiation Oncology,Biology,Physics*, 1995.

[85] M Stein, N Loberant, M Laviov, G Rennert, et al. Second cancer in patients treated for testicular seminoma. *Journal of Surgical Oncology*, 49(1):16–19, 1992.

[86] C van Walraven, D Fergusson, C Earle, N Baxter, et al. Association of diagnostic radiation exposure and second abdominal-pelvic malignancies after testicular cancer. *Journal of Clinical Oncology*, 29(21):2883–2888, 2011.

[87] TV Tarin, G Sonn, and R Shinghal. Estimating the risk of cancer associated with imaging related radiation during surveillance for stage I testicular cancer using computerized tomography. *The Journal of Urology*, 181(2):627–633, 2009.

[88] TJ Kinsella, G Trivette, J Rowland, R Sorace, et al. Long-term follow-up of testicular function following radiation therapy for early-stage Hodgkin's Disease. *Journal of Clinical Oncology*, 7(6):718–24, 1989.

[89] GM Centola, JW Keller, M Henzler, and P Rubin. Effect of low-dose testicular irradiation on sperm count and fertility in patients with testicular seminoma. *J Androl*, 15(6):608–13, 1994.

[90] M Clarke, R Collins, S Darby, C Davies, et al. Effects of radiotherapy and of differences in the extent of surgery for early breast cancer on local recurrence and 15-year survival: An overview of the randomised trials. *Lance*, 366:2087–2106, 2005.

[91] G Liljegren, L Holmberg, J Bergh, A Lindgren, et al. 10-year results after sector resection with or without postoperative radiotherapy for stage I breast cancer: A randomized trial. *Journal of Clinical Oncology*, 17(8):2326–2333, 1999.

[92] B Fisher, S Anderson, J Bryant, RG Margolese, et al. Twenty-year follow-up of a randomized trial comparing total mastectomy, lumpectomy, and lumpectomy plus irradiation for the treatment of invasive breast cancer. *New England Journal of Medicine*, 347(16):1233–1241, 2002.

[93] SEER Program (National Cancer Institute (U.S.)) and National Center for Health Statistics (U.S.). SEER cancer statistics review. 1993.

[94] CL Shapiro and A Recht. Side effects of adjuvant treatment of breast cancer. *New England Journal of Medicine*, 344(26):1997–2008, 2001.

[95] PD Inskip, M Stovall, and JT Flannery. Lung cancer risk and radiation dose among women treated for breast cancer. *Journal of the National Cancer Institute*, 86(13):983–988, 1994.

[96] JP Pignol, B Keller, and A Ravi. Doses to internal organs for various breast radiation techniques - implications on the risk of secondary cancers and cardiomyopathy. *Radiation Oncology*, 6(1):5, 2011.

[97] CW Taylor, JM Povall, P McGale, A Nisbet, et al. Cardiac dose from tangential breast cancer radiotherapy in the year 2006. *International Journal of Radiation Oncology, Biology, Physics*, 72(2):501–507, 2008.

[98] P McGale, SC Darby, P Hall, J Adolfsson, et al. Incidence of heart disease in 35,000 women treated with radiotherapy for breast cancer in Denmark and Sweden. *Radiotherapy and Oncology*, 100(2):167–175, 2011.

[99] S Johansen, KV Reinertsen, K Knutstad, DR Olsen, and SD Fosså. Dose distribution in the thyroid gland following radiation therapy of breast cancer - A retrosective study. *Radiation Oncology*, 6(68), 2011.

[100] C Giani, P Fierabracci, R Bonacci, A Gigliotti, et al. Relationship between breast cancer and thyroid disease: Relevance of autoimmune thyroid disorders in breast malignancy. *Journal of Clinical Endocrinology & Metabolism*, 81(3):990–994, 1996.

[101] J Huang, R Walker, PG Groome, W Shelley, and WJ Mackillop. Risk of thyroid carcinoma in a female population after radiotherapy for breast carcinoma. *Cancer*, 92(6):1411–1418, 2001.

[102] MP Casebow. Matching of adjacent radiation beams for isocentric radiotherapy. *British Journal of Radiology*, 57(680):735–740, 1984.

[103] WB Warlick, JH O'Rear, L Earley, JH Moeller, et al. Dose to the contralateral breast: A comparison of two techniques using the enhanced dynamic wedge versus a standard wedge. *Medical Dosimetry*, 22(3):185–191, 1997.

[104] CD Weides, EC Mok, WC Chang, DO Findley, and CA Shostak. Evaluating the dose to the contralateral breast when using a dynamic wedge versus a regular wedge. *Medical Dosimetry*, 20(4):287–293, 1995.

[105] J Yarnold, A Ashton, J Bliss, J Homewood, et al. Fractionation sensitivity and dose response of late adverse effects in the breast after radiotherapy for early breast cancer: Long-term results of a randomised trial. *Radiotherapy and Oncology*, 75(1):9–17, 2005.

[106] The START Trialist's Group. The UK standardisation of breast radiotherapy (START) trial A of radiotherapy hypofractionation for treatment of early breast cancer: A randomised trial. *The Lancet Oncology*, 9(4):331–341, 2008.

[107] HH Storm, M Andersson, JD Boice, M Blettner, et al. Adjuvant radiotherapy and risk of contralateral breast cancer. *Journal of the National Cancer Institute*, 84(16):1245–1250, 1992.

[108] R Roychoudhuri, H Evans, D Robinson, and H Møller. Radiation-induced malignancies following radiotherapy for breast cancer. *British Journal of Cancer*, 91(5):868–872, 2004.

[109] O Turken, Y NarIn, S DemIrbas, ME Onde, et al. Breast cancer in association with thyroid disorders. *Breast Cancer Research*, 5(5):R110–R113, 2003.

[110] CR Edwards and PJ Mountford. Near surface photon energy spectra outside a 6 MV field edge. *Physics in Medicine and Biology*, 49(18):N293, 2004.

[111] SB Scarboro, DS Followill, RM Howell, and SF Kry. Variations in photon energy spectra of a 6 MV beam and their impact on TLD response. *Medical Physics*, 38(5):2619–2628, 2011.

[112] CS Reft, R Runkel-Muller, and L Myrianthopoulos. In vivo and phantom measurements of the secondary photon and neutron doses for prostate patients undergoing 18 MV IMRT. *Medical Physics*, 33(10):3734–3742, 2006.

[113] P Lindsay, A Rink, M Ruschin, and D Jaffray. Investigation of energy dependence of EBT and EBT-2 Gafchromic film. *Medical Physics*, 37(2):571–576, 2010.